JGR Atmospheres

RESEARCH ARTICLE
10.1029/2024JD041812

# Emissions and Chemistry of Volatile Organic Compounds in the Los Angeles Basin in Summer 2022

**A. R. Jensen[1,2,3], M. A. Morris[1,2], B. C. Schulze[4], A. C. Bradley[1,2], L. D. Anderson[1,2], O. J. Jenks[1,2], W. D. Dresser[1,2], K. Ball[5], R. X. Ward[4], D. A. Day[1,2], J. D. Crounse[4], S. Meinardi[6], B. Barletta[6], D. R. Blake[6], J. H. Seinfeld[5], P. O. Wennberg[4,7], J. L. Jimenez[1,2], and J. A. de Gouw[1,2]**

[1]Cooperative Institute for Research in Environmental Sciences, University of Colorado, Boulder, Boulder, CO, USA, [2]Department of Chemistry, University of Colorado, Boulder, Boulder, CO, USA, [3]Now at Department of Chemistry, University of Michigan, Ann Arbor, MI, USA, [4]Division of Geological and Planetary Sciences, California Institute of Technology, Pasadena, CA, USA, [5]Division of Chemistry and Chemical Engineering, California Institute of Technology, Pasadena, CA, USA, [6]Department of Chemistry, University of California, Irvine, Irvine, CA, USA, [7]Division of Engineering and Applied Science, California Institute of Technology, Pasadena, CA, USA

**Key Points:**

- Concentrations of aromatic hydrocarbons in Los Angeles have declined since 2010 while those of oxygenated volatile organic compounds (VOCs) are similar or higher
- Midday photochemistry was ~68% faster in 2022 than 2010 possibly due to higher average temperatures and changes in the $NO_x$-VOC regime
- Ozone concentrations were similar between 2010 and 2022 due to the combination of changes in emissions, photochemistry, and meteorology

**Supporting Information:**

Supporting Information may be found in the online version of this article.

**Correspondence to:**

J. A. de Gouw,
Joost.deGouw@Colorado.edu

**Citation:**

Jensen, A. R., Morris, M. A., Schulze, B. C., Bradley, A. C., Anderson, L. D., Jenks, O. J., et al. (2024). Emissions and chemistry of volatile organic compounds in the Los Angeles basin in summer 2022. *Journal of Geophysical Research: Atmospheres*, *129*, e2024JD041812. https://doi.org/10.1029/2024JD041812

Received 15 JUN 2024
Accepted 13 DEC 2024

**Author Contributions:**

**Conceptualization:** P. O. Wennberg, J. L. Jimenez, J. A. de Gouw
**Data curation:** A. R. Jensen, J. D. Crounse, S. Meinardi, B. Barletta, P. O. Wennberg
**Formal analysis:** A. R. Jensen, S. Meinardi
**Funding acquisition:** D. R. Blake, P. O. Wennberg, J. L. Jimenez, J. A. de Gouw
**Investigation:** A. R. Jensen, M. A. Morris, B. C. Schulze, A. C. Bradley, L. D. Anderson, O. J. Jenks, W. D. Dresser, K. Ball, R. X. Ward, D. A. Day, J. D. Crounse, S. Meinardi, B. Barletta, P. O. Wennberg, J. L. Jimenez, J. A. de Gouw
**Methodology:** A. R. Jensen, M. A. Morris, D. A. Day, J. D. Crounse, S. Meinardi,



**Abstract** The ozone air quality standard is regularly surpassed in the Los Angeles air basin, and efforts to mitigate ozone production have targeted emissions of precursor volatile organic compounds (VOCs), especially from mobile sources. In order to assess how VOC concentrations, emissions, and chemistry have changed over the past decade, VOCs were measured in this study using a Vocus-2R proton-transfer reaction time-of-flight mass spectrometer in Pasadena, California, downwind of Los Angeles, in summer 2022. Relative to 2010, ambient concentrations of aromatic hydrocarbons have declined at a similar rate as carbon monoxide, suggesting reduced overall emissions from mobile sources. However, the ambient concentrations of oxygenated VOCs have remained similar or increased, suggesting a greater relative importance of oxidation products and other emission sources, such as volatile chemical products whose emissions are largely unregulated. Relative to 2010, the range of measured VOCs was expanded, including higher aromatics and additional volatile chemical products, allowing a better understanding of a wider range of emission sources. Emission ratios relative to carbon monoxide were estimated and compared with 2010 emission ratios. Average measured ozone concentrations were generally comparable between 2022 and 2010; however, at the same temperature, daytime ozone concentrations were lower in 2022 than 2010. Faster photochemistry was observed in 2022, with average hydroxyl radical exposure being ~68% higher during midday (statistically significant at 95% confidence), although this difference reduces to ~35% when comparing observations at ambient temperatures of 25–30°C only. Future trends in temperature are important in predicting ozone production.

**Plain Language Summary** Gas-phase organic molecules are emitted from many sources including vegetation, cars, cooking, industries, and chemical products (paints, inks, pesticides, deodorant, shampoo, etc.), among others. These emissions oxidize in the atmosphere and contribute to the formation of particles and ozone, which are harmful to human health. To improve air quality, the behavior of these molecules in the atmosphere must be understood, and their sources must be identified, before effective emission reduction policies can be established. In summer 2022, we measured atmospheric concentrations of such molecules in Pasadena, California, downwind of Los Angeles, California, to investigate fresh, unreacted emissions as well as aged, oxidized emissions. Compared to similar measurements made in 2010, emissions from vehicle sources appear to have declined while chemical products have become relatively more important. Atmospheric oxidation of these emissions also appears to have increased relative to 2010, in part due to higher average temperatures and related meteorology. Despite reduced emissions from vehicles, unregulated emissions from chemical products and faster oxidation yielded similar concentrations of secondary products such as ozone. Future air quality improvements will likely require further emission reductions, particularly for chemical products, and such improvements may be offset by rising temperatures due to climate change.

## 1. Introduction

The Los Angeles (LA) basin in California is home to more than 15 million people and regularly exceeds the National Ambient Air Quality Standard (NAAQS) for ozone (Fujita et al., 2013; US EPA, 2023). Ozone, which is hazardous to respiratory health (Chen et al., 2007; Nuvolone et al., 2018), is produced via the oxidation of volatile

B. Barletta, D. R. Blake, J. L. Jimenez, J. A. de Gouw
**Project administration:** D. R. Blake, P. O. Wennberg, J. L. Jimenez, J. A. de Gouw
**Resources:** A. R. Jensen, M. A. Morris, A. C. Bradley, L. D. Anderson, O. J. Jenks, W. D. Dresser, D. A. Day, J. D. Crounse, S. Meinardi, B. Barletta
**Supervision:** B. Barletta, D. R. Blake, J. H. Seinfeld, P. O. Wennberg, J. L. Jimenez, J. A. de Gouw
**Validation:** A. R. Jensen, S. Meinardi
**Visualization:** A. R. Jensen, J. A. de Gouw
**Writing – original draft:** A. R. Jensen, J. A. de Gouw
**Writing – review & editing:** A. R. Jensen, M. A. Morris, B. C. Schulze, A. C. Bradley, L. D. Anderson, O. J. Jenks, W. D. Dresser, K. Ball, R. X. Ward, D. A. Day, J. D. Crounse, S. Meinardi, B. Barletta, D. R. Blake, J. H. Seinfeld, P. O. Wennberg, J. L. Jimenez, J. A. de Gouw

organic compounds (VOCs) in the presence of nitrogen oxides ($NO_x \equiv NO + NO_2$) and sunlight (Chameides et al., 1992; Derwent et al., 1996; Jacob, 1999). However, reductions in precursor emissions have not necessarily yielded net improvements in ozone concentrations due to the nonlinear chemistry (Fujita et al., 2013; Nussbaumer & Cohen, 2020; Pollack et al., 2013; Warneke et al., 2013) and the strong dependence of ozone on temperature combined with a warming climate (Nussbaumer & Cohen, 2020; Pusede et al., 2015).

The COVID-19 pandemic in 2020 provided an extreme test-case of our understanding of emissions: the stay-at-home order restricted non-essential activities and the associated emissions were reduced on a global scale. In LA, ambient $NO_x$ concentrations were estimated to be ∼30%–40% lower due to the stay-at-home orders (Goldberg et al., 2020; H. Parker et al., 2020) while ambient concentrations of VOCs demonstrated insignificant reductions (Van Rooy et al., 2021). Despite these perturbations, the stay-at-home orders caused only minor average ozone reductions of 0–2 ppbv (Schroeder et al., 2022) with enhancements downwind of regions with the highest population densities (H. Parker et al., 2020; L. Parker et al., 2022). Recent studies suggest that the LA basin is near the transition point from a $NO_x$-saturated regime to a $NO_x$-limited regime such that further reductions of $NO_x$ emissions may result in reduced ozone production and NAAQS attainment (Kim et al., 2022; Nussbaumer & Cohen, 2020; Schroeder et al., 2022; Zhu et al., 2022). Even in a $NO_x$-limited regime, future air quality improvements will rely on further emission reductions of both $NO_x$ and VOCs.

Traditional measures to reduce emissions and improve air quality have targeted the transportation and industrial sectors (National Research Council, 2004). In recent decades, ambient concentrations of precursor VOCs and $NO_x$ have declined in response to such measures (McDonald et al., 2012; Wallington et al., 2022; Warneke et al., 2012), contributing to improved health and air quality (Garcia et al., 2023; Parrish et al., 2016). However, the declining importance of mobile VOC sources has increased the relative importance of other sources, including those associated with the use of volatile chemical products (VCPs; paints, inks, adhesives, pesticides, cleaning agents, personal care products, etc.). Despite making up only ∼4% of petrochemical product use in LA (with the other 96% consisting of fossil-fuel transportation and heating fuels), VCPs are estimated to account for ∼38% of the total VOC emissions and ∼46% of the VOC reactivity (McDonald et al., 2018). Ambient observations support these estimates for a broader range of urban environments (Gkatzelis, Coggon, McDonald, Peischl, Gilman, et al., 2021) and other studies have demonstrated significant VCP contributions to urban ozone production (Coggon et al., 2021; Seltzer et al., 2021). Cao et al. (2023) observed enhanced evaporative emissions in New York City during an abnormally warm spring, suggesting that the warming climate may offset air quality improvements made through reducing VOC emissions from mobile sources. Wu et al. (2024) note that knowledge of temperature-dependent evaporative emissions is necessary to fully characterize ozone pollution. New policies are needed to address this transition from mobile sources to VCPs and possibly other sources as the dominant contributors of anthropogenic VOCs to the urban atmosphere.

Ambient VOC measurements can improve our scientific understanding and help inform policy through quantification of precursor emissions and photochemical product formation. The measured atmospheric composition is affected by many emission sources, both local and regional. Additionally, different species' lifetimes range from days to hours or less, so emissions have undergone transport, dilution, and chemical transformation by the time they are measured. In some studies, emission compositions have been compared through the calculation of emission ratios after also accounting for removal and/or formation (Borbon et al., 2013; de Gouw et al., 2005, 2017, 2018; Warneke et al., 2007). Technological advancements, as in the case of Tofwerk's Vocus focusing ion-molecule reactor (Krechmer et al., 2018) and high mass resolution time-of-flight mass spectrometry (Graus et al., 2010; Jordan et al., 2009; Yuan et al., 2016), have allowed for the measurement of a wider range of VOCs with lower limits of detection. These capabilities allow for an improved characterization of VOC emissions and chemical transformations.

In this paper, we describe VOC measurements made by a Vocus-2R proton-transfer reaction time-of-flight mass spectrometry (PTR-TOF-MS) in Pasadena, California, downwind of LA during the California Research at the Nexus of Air Quality and Climate Change-Two field campaign (CalNexT-2022), a follow-up study to the CalNex-2010 campaign (Ryerson et al., 2013). We discuss changes in ambient concentrations of criteria pollutants, primary VOCs, and secondary VOCs, as well as exposure to hydroxyl radicals, to assess general emission and oxidation trends relative to CalNex-2010 and the Los Angeles Air Quality Campaign (LAAQC-2020). We also quantify and compare the emission ratios of these VOCs and extend this analysis to additional species such as polycyclic aromatic hydrocarbons and cyclic volatile methyl siloxanes. We then present a more exploratory

analysis of all measured signals to compare the measurement results during the day and night. Finally, we discuss observations made with an oxidation flow reactor and their implications for ambient oxidation.

## 2. Measurements

### 2.1. Sampling Location

Measurements were made from 30 June–14 August 2022. Ambient air was sampled from a mechanical room on the roof of Caltech Hall in Pasadena, California, USA (34.136800°N, 118.126209°W) with an inlet height of ∼40 m above ground level. This sampling location differs from that from CalNex-2010 (which was ∼0.5 km to the northeast), such that the two sites may be sampling slightly different local emissions (discussed further in Section 3.1). Definitions for nighttime (22:00–06:00 Pacific Daylight Time (PDT)) and daytime (10:00–18:00 PDT) were adopted from de Gouw et al. (2017, 2018).

Historical and present meteorological measurements were obtained from the TCCON weather station on the roof of the Ronald and Maxine Linde Laboratory (∼10 m above ground level; 34.136363°N, 118.126817°W), which neighbors Caltech Hall (TCCON Weather, 2022).

### 2.2. On-Line VOC Measurements

VOCs were measured by a Vocus-2R proton-transfer-reaction time-of-flight mass spectrometer (PTR-TOF-MS; Tofwerk AG and Aerodyne Research, Inc.), hereafter referred to as the Vocus, which is detailed elsewhere (Krechmer et al., 2018). Briefly, reagent ions, hydronium, are formed in a discharge ion source before reaction with the sampled air stream. Proton-transfer takes place between the primary ion and analyte VOC to form a product ion, provided the proton affinity of that VOC is greater than that of water. Most VOCs with unsaturated bonds or heteroatoms can be measured with this technique. Itis worth noting that smaller alkanes, ethene, and ethyne have low proton affinities and are not detected by PTR. Larger alkanes' proton affinities increase with size, approaching or surpassing that of water (Fu et al., 2022), but the ionization is inefficient and detection is further affected by fragmentation (Gueneron et al., 2015).

The Vocus utilizes a focusing ion-molecule reactor (FIMR) with both axial and radial electric fields. The constant axial field along the FIMR enhances ion collision energies to reduce the formation of water clusters and promote simple reaction kinetics. The radial field is applied by a radio frequency quadrupole mounted outside the FIMR. This quadrupole focuses ions to the central axis of the FIMR, thereby improving ion transmission and sensitivities. The FIMR in this study was operated at 90°C and 1.5 mbar with 480 and 400 V for the axial and quadrupole voltages, respectively, for a reduced electric field strength ($E/N$) of 160 Td. In between the FIMR and the time-of-flight mass analyzer, a radio frequency quadrupole ion guide (255 V amplitude) not only transports the ions but also attenuates the hydronium ion signal, which increases the lifespan of the detector. For the measurement period, the mass resolution ($m/\Delta m$ FWHM) was ∼8,000 for $C_8H_{10}H^+$ (mass-to-charge ratio, $m/z$, 107). With typical operation and optimization, mass resolution can be as high as ∼10,000 in the Vocus. However, limited time in the field for instrument optimization resulted in this lower resolution, which was still sufficient to separate most ions of interest.

Ambient air was sampled via a 2.8-m perfluoroalkoxy alkane (PFA) Teflon line (0.64 cm OD; 0.38 cm ID) with a bypass flow rate of 2,620 ± 40 $cm^3$ $min^{-1}$ at standard temperature and pressure (sccm; STP defined as 298 K and 1 atm). Mass spectra from $m/z$ 4–398 were recorded at a 1 Hz time resolution. Analyses including high resolution peak fitting of mass spectra (Cubison & Jimenez, 2015; Timonen et al., 2016) and TOF duty cycle corrections (relative to $m/z$ 59) were performed using Tofware (v3.2.5; Tofwerk AG and Aerodyne Research, Inc.) in the Igor Pro 9 environment (WaveMetrics, OR, USA). In addition to ambient sampling, ambient air was also sampled downstream of an oxidative flow reactor (OFR) and a gas chromatograph (GC). These different measurements are detailed in the following sections. To differentiate the measurements, the real-time measurements are denoted as RT-Vocus. All sample lines maintained constant flows regardless of the sampled channel to limit inlet delays.

### 2.3. RT-Vocus Instrument Background Measurements

RT-Vocus instrument background measurements were made for 2 min at 40 min intervals. Ambient air was passed through a catalytic zero air generator (Tofwerk AG) and then used to overflow the Vocus inlet. This catalyst was found to produce lower instrument background signals than a hydrocarbon trap and UHP nitrogen

(Jensen et al., 2023). In addition to these short, frequent measurements, longer measurements were made daily to determine limits of detection (LODs). The inlet was first flushed for 5 min, and then measurements were made for an additional 5 min.

### 2.4. RT-Vocus Calibrations

RT-Vocus sensitivities were determined in the field by calibration of a standard mixture containing 13 VOCs (Apel-Riemer Environmental, Inc.; Table S1 in Supporting Information S1; nominally 1 ppmv each except β-caryophyllene, which was 0.1 ppmv). Two methods were used for calibrations: fast, frequent calibrations, as well as multipoint calibrations. Fast calibrations consisted of a single dilution of nominally 6.5 ppbv and were made for 2 min at 80 min intervals, coinciding with every other instrument background measurement. Multipoint calibrations were performed daily to verify the fast calibrations. The multipoint calibrations consisted of 5 dilutions, nominally 4–7.5 ppbv, plus an instrument background measurement. The two kinds of calibration agreed within ∼5%. The fast sensitivities were linearly interpolated in the analysis of data.

Additional standard mixtures were used in the laboratory for calibration of additional VOCs. Field sensitivities for these standards were estimated by assuming a similar proportionality between the field and laboratory sensitivities of the field-deployed standard mixture. This proportionality and estimated sensitivities were determined for each fast calibration. Table S2 in Supporting Information S1 summarizes the sensitivities and limits of detection obtained for these additional standards.

For compounds that are not contained in any of the calibration standards, we use calculated sensitivities based on their reaction rate coefficients ($k_{PTR}$), *m/z*, and a characterization of the instrument. Values of $k_{PTR}$ were estimated for the above reactor conditions using molecular polarizabilities and permanent dipole moments (Chesnavich et al., 1980; Langevin, 1905; Su, 1994; Su & Chesnavich, 1982). These parameters were taken from the literature where available (Cappellin et al., 2010, 2012; Haynes, 2014; Langford et al., 2013; Zhao & Zhang, 2004), or otherwise estimated using the framework established by Sekimoto et al. (2017) based on molecular formulas and properties.

The field and laboratory calibrations were used to characterize the instrument and calibrate for species not contained in any of our standards. This characterization was done on the 80-min time scale of the fast calibrations using the PTR Data Toolkit version 1.0 (Jensen et al., 2023). This characterization was used in place of typical normalization against the reagent ion due to the high mixing ratio of water in the FIMR and the instrument's insensitivity to relative humidity (Jensen et al., 2023; Krechmer et al., 2018).

Observed sensitivities were also corrected for fragmentation. Fragmentation patterns were determined from GC measurements for resolved compounds. Contributions from the parent ion and its fragments were corrected for transmission efficiencies and isotopic distributions as discussed by Jensen et al. (2023).

Quantification of three specific compounds was done differently to account for interferences: acetaldehyde, isoprene, and benzene. Acetaldehyde's quantitative ion, $C_2H_4OH^+$, had interfering contributions from ethanol. This ion has been observed for selected ion flow tube mass spectrometry measurements of ethanol with $O_2^+$ as the reagent ion (Španěl & Smith, 1997). The additional signal from ethanol was subtracted in a similar manner as presented by Coggon, Stockwell, Claflin, et al. (2024) and Coggon, Stockwell, Xu, et al. (2024). The ratio between the parent and fragment ions of ethanol was determined using the ambient GC chromatograms. This ratio was used to scale ethanol's quantitative ion ($C_2H_6OH^+$) signal, and this estimated interference was then subtracted from the acetaldehyde signal. The interference from ethanol accounted for 32 ± 9% (average and 1 standard deviation) and 17 ± 5% of the nighttime and daytime $C_2H_4OH^+$ ambient signals, respectively (Figure S1 in Supporting Information S1).

Isoprene's quantitative ion, $C_5H_8H^+$, had contributions from several peaks in the chromatograms (Figures S2a and S2b in Supporting Information S1) which has been reported previously (Coggon, Stockwell, Claflin, et al., 2024; Vermeuel et al., 2023; Yuan et al., 2017). The peaks' corresponding parent ions are identified primarily as *n*-aldehydes (*n*-pentanal, *n*-octanal, and *n*-nonanal; no significant contributions were observed from *n*-hexanal, nor *n*-heptanal) due to their significant fragmentation (Buhr et al., 2002; Pagonis et al., 2019). Cycloalkanes have also been observed as fragmenting to yield the $C_5H_8H^+$ ion (Coggon, Stockwell, Claflin, et al., 2024; Gueneron et al., 2015). We employed a similar correction as described by Coggon, Stockwell, Claflin, et al. (2024) and Coggon, Stockwell, Xu, et al. (2024). The real-time signal of $C_5H_8H^+$ was regressed against the signals of the

protonated aldehydes and their respective dehydration products for nighttime data when isoprene had negligible contributions to the $C_5H_8H^+$ chromatograms (Figure S2c in Supporting Information S1). The dehydration product of *n*-nonanal, $C_9H_{17}^+$, yielded the highest correlation ($r^2 = 0.95$), so it was used as a proxy for all *n*-aldehydes, which were assumed to trend together in time. This ion also corresponds to fragments of substituted cycloalkanes (Gueneron et al., 2015; Warneke et al., 2014), allowing for the simultaneous correction for these cycloalkanes (Coggon, Stockwell, Claflin, et al., 2024). It is worth noting that $C_9H_{17}^+$ had the highest signal of the *n*-aldehyde and dehydration product ions considered here. The slope of the nighttime regression ([$C_5H_8H^+$ cps] [$C_9H_{17}^+$ cps]$^{-1}$) and the real-time $C_9H_{17}^+$ signal were used to correct the isoprene signal for the interference from aldehydes in a similar manner as done with acetaldehyde. This correction was substantial, making up 110 ± 20% and 30 ± 13% of the nighttime and daytime $C_5H_8H^+$ ambient signals, respectively (Figure S2d in Supporting Information S1). Biogenic isoprene emissions are light-dependent (Sanadze, 2004) and reactive (Kurpius & Goldstein, 2003; Wolfe et al., 2011), resulting in near-zero nighttime concentrations. However, there are also anthropogenic isoprene emissions (Borbon et al., 2023; Coggon, Stockwell, Claflin, et al., 2024; Peron et al., 2024), which are confirmed by small, but nonzero chromatographic peaks for nighttime isoprene. The above correction assumes essentially zero nighttime isoprene and overcorrects the nighttime data.

Finally, benzene was quantified using its $O_2^+$ charge-transfer product, $C_6H_6^+$, which has been found to be more selective (Coggon, Stockwell, Claflin, et al., 2024). The charge transfer product is more unique to benzene whereas ethylbenzene and benzaldehyde commonly fragment to $C_6H_6H^+$, the proton-transfer product for benzene. No other chromatographic peaks were observed for the $C_6H_6^+$ ion. This charge-transfer product was calibrated directly during the field calibrations on an 80 min timescale (i.e., this quantification did not involve a correction, but rather a different quantitative ion). Variability in the $O_2^+$ ion chemistry between calibrations may have influenced benzene signal. The ratio of charge-transfer to PTR benzene sensitivities ($C_6H_6^+/C_6H_6H^+$) was initially elevated (~0.5–0.75) during the first week following instrument setup, but settled to 0.26 ± 0.01 for the remainder of the campaign.

### 2.5. Gas Chromatography

Speciation and fragmentation were determined using an Aerodyne Research Inc. GC interfaced with the Vocus (GC-Vocus). A prototype of this instrument was described by Claflin et al. (2021), and Vermeuel et al. (2023) described a similar instrument as used in this study. Briefly, the GC system employs a dual-stage thermal desorption preconcentrator (TDPC) consisting of a multi-bed adsorbent sample trap (C3-BAXX-5070; Markes International) followed by a multi-bed adsorbent focus trap (U-T15ATA; Markes International) to improve chromatographic resolution. Two columns were used in this study and were swapped every other week: a Restek MXT-624 column (30 m, 0.25 mm ID, 1.4 μm film thickness), which resolves non-polar to mid-polarity compounds, and a Restek MXT-WAX column (30 m, 0.25 mm ID, 0.25 μm film thickness), which resolved more polar and higher molecular-weight compounds.

Samples were collected off the main Vocus sample line ahead of the Vocus inlet (additional 1.4 m PFA; bypass line flow rate of 1,600 ± 30 sccm) immediately before the start of each cycle. To remove reactive gasses such as ozone and mitigate sampling artifacts, samples were first passed through a quartz tube with anhydrous sodium sulfite held in place with silanized glass wool on either side (Helmig, 1997). These oxidant-scrubbed samples were then immediately directed toward and collected onto the sample trap at 20°C for 10 min at a flow rate of 100 sccm for sample volume of 1 L at STP.

GC measurements (20 min) were performed once every 5 hr, starting with a heated backflush of the column. Trapped water was reduced by purging the sample in the sample trap (20°C) for 2 min with ultrahigh purity (UHP) nitrogen (Airgas). Samples were then transferred via UHP helium (Airgas) to the focus trap, and then to the column by flash heating the traps to 300°C in sequence. Chromatograms were obtained using a programmed temperature ramp from 35 to 235°C over ~10 min and a UHP helium flow rate of 3 sccm. The effluent was diluted into 250 sccm of air from the catalytic zero air generator before overflowing the Vocus sample inlet to meet the minimum flow required by the Vocus.

During GC runs, mass spectra were recorded at a frequency of 5 Hz. Following high resolution peak fitting in Tofware, chromatographic peaks were analyzed using the TERN software package (v2.2.19; Aerodyne Research, Inc.) (Isaacman-VanWertz et al., 2022; Lerner et al., 2017) in the Igor Pro 8 environment where peak areas were determined by fitting to modified Gaussian curves (Isaacman-VanWertz et al., 2017).

The same standard mixture of 13 VOCs (Table S1 in Supporting Information S1) was used every other day to calibrate the set-up at nominally 4 ppbv (diluted by a factor of 250 from the standard mixture) and instrument backgrounds were measured daily. Multipoint calibrations from 0 to 12.8 ppbv (five dilutions plus an instrument background measurement; each in triplicate) were performed using the field and laboratory standard mixtures after the measurement period. UHP nitrogen was used for all field and laboratory instrument background measurements and dilutions.

### 2.6. Oxidation Flow Reactor

An oxidation flow reactor (OFR) was used to oxidize ambient air in situ, mimicking the hydroxyl radical (OH) and ozone oxidation processes in LA during the day. The reactor turns VOC precursors into more oxidized products, which may then undergo gas-to-particle partitioning, with limited wall effects (Brune, 2019). The Vocus was used to observe the transformation of VOC precursors into products (OFR-Vocus). The design, premise, and chemistry are described in detail elsewhere (Kang et al., 2007; Lambe et al., 2011; R. Li et al., 2015; Ortega et al., 2016; Peng & Jimenez, 2020). Briefly, ambient air was sampled directly into the cylindrical, aluminum reactor (~13 L) via a 14 cm diameter opening at a rate of 4.4 L $min^{-1}$ without inlet tubing (referred to as the "ambient OFR" in the campaign), corresponding to a residence time of ~3 min. The opening included a coarse-grid mesh screen coated with an inert silicon coating (Sulfinert by SilcoTek, Bellefonte, PA) designed to block debris and break up large eddies. Narrow-band ultraviolet light (254 and 185 nm) was emitted by two low-pressure mercury lamps (model 82-9304-03, BHK Inc.) and initiated oxygen, water, and ozone photochemistry. This mode of operation, referred to as OFR185, produces ozone by $O_2$ photolysis as well as OH from ambient water vapor and ozone photolysis (R. Li et al., 2015; Peng & Jimenez, 2020). However, the ratio of ozone to OH is similar to ambient conditions, and OH chemistry is dominant over direct photolysis and other radical chemistry ($O(^1D)$ + VOC, etc.) for all VOCs (Peng et al., 2016). There may be photolysis exceptions for some VOCs There may be a few VOCs with very high absorption cross sections at 254 nm, for which the photolysis contribution may reach 10%–20% (Peng et al., 2016). The lamp intensities were controlled to adjust radical production and OH exposure, with a target exposure of ~1–2 days (referenced to an average OH concentration of $1.5 \times 10^6$ molecules $cm^{-3}$) (Mao et al., 2009), which has been observed in past studies to maximize secondary organic aerosol (SOA) formation from ambient air (Ortega et al., 2016). The Vocus sampled 1.1 m downstream of the OFR with a bypass flow rate of 1,020 ± 11 sccm. The flow rate through the OFR was kept constant whether the Vocus was sampling it or not, by adjusting bypass flow rates.

### 2.7. Supplemental Measurements

Additional particle and trace gas measurements were made alongside the Vocus as part of the California Institute of Technology Air Quality Station including nitrogen monoxide (NO; Teledyne T200U), nitrogen dioxide ($NO_2$; Teledyne T500U), carbon monoxide (CO; Teledyne M300EU2), and ozone (Teledyne T400).

Whole air samples (WAS) were collected in a similar manner as described by Van Rooy et al. (2021). Briefly, hour-integrated samples were collected into 2-L electropolished canisters to 20 psi using a 32-canister auto-sampler (Atmospheric Technology Model 8001). Three samples were collected each day from 3 March to 15 August 2022: 05:30–06:30, 09:00–10:00, and 14:00–15:00 PDT. Additional samples were collected hourly from midnight on 1 July to 23:00 on 1 August to construct a diurnal profile. Analysis was performed at the University of California, Irvine (UCI) as described in greater detail elsewhere (Colman et al., 2001). Briefly, a multi-column, multi-detector (flame ionization, electron capture, and quadrupole mass spectrometry) GC system (Hewlett-Packard 6890 GC units) was used to identify and quantity a suite of trace gases.

Intercomparisons were made between the RT-Vocus and UCI WAS samples (Figure S3 in Supporting Information S1). Aromatic hydrocarbons had good agreement within ~30% and strong correlations ($r^2 \geq 0.93$) except for styrene. GC-Vocus chromatograms show strong contributions to styrene's quantitative ion ($C_8H_8H^+$) from the fragmentation of C8 and C9 aromatics, so we avoid a detailed analysis of styrene data. RT-Vocus measurements of dimethyl sulfide (DMS) were much greater than those from the UCI WAS measurements. DMS was calibrated in the laboratory and its sensitivity relative to other field standards agrees with the relative sensitivity reported elsewhere for Vocus measurements of DMS (Kilgour et al., 2024). Additionally, no other contributions to the DMS quantitative ion, $C_2H_6SH^+$, were observed in the GC-Vocus chromatograms. Otherwise, we do not know the cause for this discrepancy. The campaign average concentrations of DMS from CalNex-2010 (~10 part-per-

trillion by volume, pptv; in situ GC-MS) fall between those of the RT-Vocus (~26 pptv) and UCI WAS (~4 pptv) CalNexT measurements. The corrected RT-Vocus and UCI WAS measurements of isoprene also correlated well ($r^2$ = 0.99), although the RT-Vocus measurements were typically 40% higher even after the corrections (Section 2.4). For monoterpenes, only α- and β-pinene are presently reported for the UCI WAS measurements, so the RT-Vocus monoterpenes measurements are greater. While some isomers may be abundant in the urban atmosphere, for example, biogenic and anthropogenic emissions of limonene (Gu et al., 2024), the dominant monoterpenes observed by GC-Vocus were α- and β-pinene. As such, the factor-of-five observed difference is not fully explained by the lack of other monoterpene isomers in the UCI measurements. Fragmentation of other species to the quantitative ion used for monoterpenes ($C_{10}H_{16}H^+$) were not observed on the GC-Vocus, but larger, unresolved species may have made such contributions. We do not attempt to reconcile these differences here as DMS and monoterpenes are not used in this analysis.

## 3. Results and Discussion

### 3.1. Ambient Concentrations of Precursors

Average mixing ratios of primary pollutants were lower in 2022 relative to 2010. For example, the average diurnal profiles for CO, benzene, and C9 aromatics show lower concentrations at all times of day (Figure 1). Ambient concentrations of $NO_x$ were generally comparable at night and during the early morning, but lower in the early afternoon when photochemistry is fastest (Figure 1b). Both profiles for benzene show roughly constant concentrations at night when emissions drive ambient concentrations in the absence of photochemistry. Benzene concentrations in 2010 peaked in the early afternoon, whereas no daytime peak was present in 2022. C9 aromatics generally had constant nighttime concentrations followed by removal beginning in the morning with the start of photochemistry, although a greater fraction of C9 aromatics were removed in 2022 during the day compared to 2010. Compared to 2010, emissions of isoprene in 2022 seemed to increase more rapidly in the early morning and concentrations in 2022 remained high further into the evening. These observations for isoprene may reflect conditions more conducive to emissions in 2022 (e.g., higher morning temperatures in 2022, a lack of cloud cover in 2022 and greater light intensity) or generally more vegetation in close vicinity to the measurement location. The relative importance of biogenic VOC emissions for urban air quality is expected to grow with urban greening programs (Gu et al., 2021).

The observed differences in the behaviors of benzene and C9 aromatics between 2010 and 2022 may stem from emissions, meteorology, and/or photochemistry, as well as the difference in sampling location and time of year. Lower nighttime concentrations of these precursors suggest reduced emissions in 2022. Exposure of fresh emissions to higher hydroxyl radical (OH) concentrations before being sampled will remove a greater portion of the precursors. The similarities in temporal behavior of benzene and CO for each year suggest that the lack of daytime peak in 2022 was driven by changes in meteorology or emissions rather than photochemistry. Since meteorological factors should influence benzene and C9 aromatics in a similar manner, the greater daytime reduction of C9 aromatics compared to benzene between 2022 and 2010 suggests faster photochemistry. OH exposure is discussed further in Section 3.2. Alternatively, a recent study has shown that cold start emissions dominate light duty passenger vehicle emissions, such that 45 km of driving with a warm catalytic converter is necessary to match the initial cold start emissions (Drozd et al., 2016). Wernis et al. (2022) describe morning enhancements in gasoline-related hydrocarbons due to the morning commute combined with cooler temperatures and cold start emissions. They observed much lower concentrations of gasoline-related hydrocarbons later in the day, which they attributed to dilution, photochemistry, and catalytic converters, which were warmer in the afternoon than the morning.

The sampling locations in 2010 and 2022 are another possible contributor to the observed differences. In 2010, air was sampled from a small walk-up tower (~10 m) in the northeastern corner of the campus and closer to Interstate-210. In 2022, air was sampled at a height of ~44 m and at a more central location on campus. It is possible that the transport of emissions from the I-210 corridor may have led to overestimated mixing ratios of VOCs from mobile sources in 2010 and/or the structure and break-up of the shallow, nocturnal boundary layer may have led to underestimated mixing ratios relative to the ground level in 2022. Additionally, the sample inlets in 2010 were near mature trees, possibly enhancing the biogenic hydrocarbon signals such that they were not representative of the wider region and contributing to the observed differences relative to 2022. The 2010 data represent speciated GC measurements, whereas the 2022 isoprene measurements were corrected for interferences,

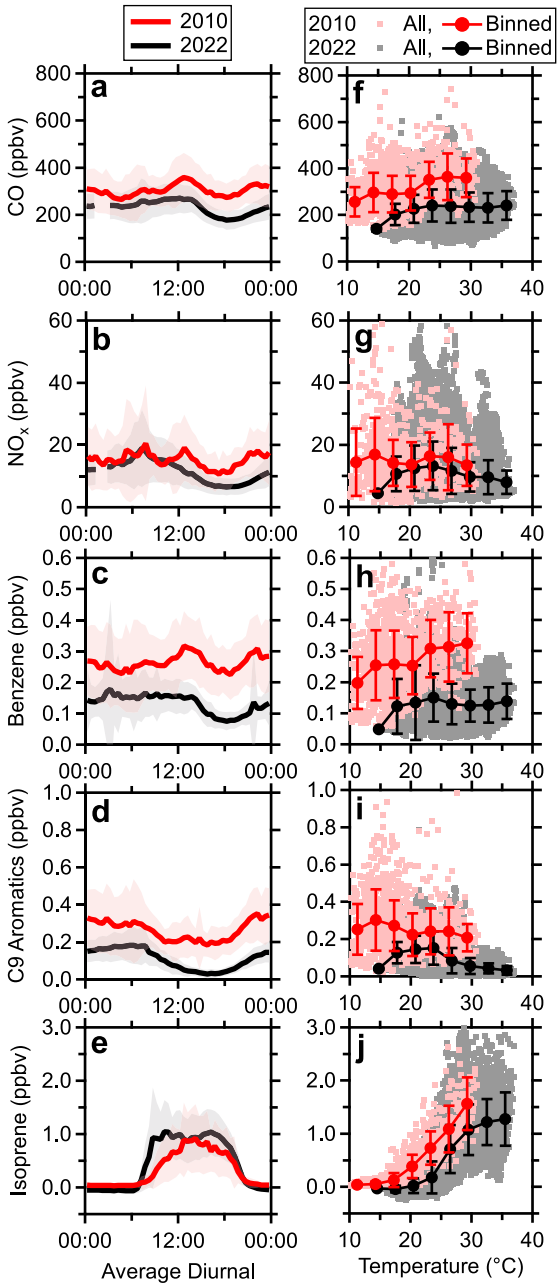


**Figure 1.** Mixing ratio diurnal averages (a–e) and mixing ratio trends with temperature during all times of day (f–j) for selected primary compounds in 2010 and 2022. Diurnal averages (a–e) represent 30-min bins and shaded regions are one standard deviation. Mixing ratios in (f–j) were averaged by temperature bins (10–40°C; 3°C bins) where the error bars denote one standard deviation. For clarity, the average markers in (f–j) are horizontally offset from the center of the temperature bins. The 2022 mixing ratios are averaged to 1 min.

as discussed in Section 2.4, which contributed to greater uncertainties in the isoprene mixing ratios. There are few emission sources between the two sites and both sites are primarily impacted by emissions on the broader scale of the LA basin.

To investigate the influence of time of year on the observed photochemistry in 2010 versus 2022, the modeled photolysis rates for $NO_2$ were compared (parameterized relative to solar zenith angle (Jenkin et al., 1997; Saunders et al., 2003); calculation described in Text S1 in Supporting Information S1). No significant differences were observed (Figure S4 in Supporting Information S1) as both studies were similarly spaced before (CalNex-2010; 15 May–15 June 2010) and after (CalNexT-2022; 30 June–14 August 2022) the summer solstice (June 21 in both years). However, the CalNex-2010 measurements experienced frequent cloud cover, reducing the measured $NO_2$ photolysis rate on affected days (Fig. S4 in Supporting Information S1). The 2022 measurements experienced near-zero cloud cover for the full measurement period, but no photolysis rates were measured for comparison with the 2010 data.

Another factor to consider is the difference in temperatures: the average daytime temperature was ~6.5°C warmer during the 2022 measurements than during the 2010 measurements (Fig. S5a in Supporting Information S1). Greater biogenic and anthropogenic VOC emissions have been found to coincide with higher temperatures (Cao et al., 2023; Khare et al., 2020; Pfannerstill et al., 2024; Wu et al., 2024). Additionally, these higher temperatures in 2022 may have affected planetary boundary layer height (PBLH) and daytime dilution, as well as potentially other changes in horizontal air circulation within the LA basin, contributing to the observed lower concentrations. It should be noted that warmer temperatures were actually associated with lower daytime PBLHs in 2010 (Figure S5b in Supporting Information S1), resulting in reduced dilution of emissions. Although the complex relationship between temperature and meteorology in the Los Angeles basin warrants further investigation for an improved interpretation of air pollution, the lower concentrations of precursors observed in 2022 suggest reduced precursor emissions in 2022. The role of temperature, as a proxy for other such influencing factors including photochemistry, is explored in Figures 1f–1j by binning the mixing ratios in 2010 and 2022 by ambient temperature. For all overlapping temperature bins and assuming similar meteorological and photochemical conditions for these bins, the concentrations of precursors are generally lower in 2022 than 2010. Although temperature does not seem to be the root cause for lower ambient concentrations, other meteorological effects, such as changes in horizontal flow patterns, may contribute. This study does not attempt to reconcile these factors, but Section 3.3 continues to explore emissions of precursors via emission ratios.

### 3.2. OH Exposure

To describe losses of reactive hydrocarbons, the OH exposure ($[OH]\Delta t$) of each air mass was calculated. OH exposure is the time-integrated exposure of emissions to OH, and is a measure of atmospheric aging that can be estimated using hydrocarbon ratios as done in previous studies (Borbon et al., 2013; de Gouw et al., 2017; Ensberg et al., 2014; Hayes et al., 2013). Equation 1 shows the dependence of OH exposure on the logarithm of the hydrocarbon ratios:

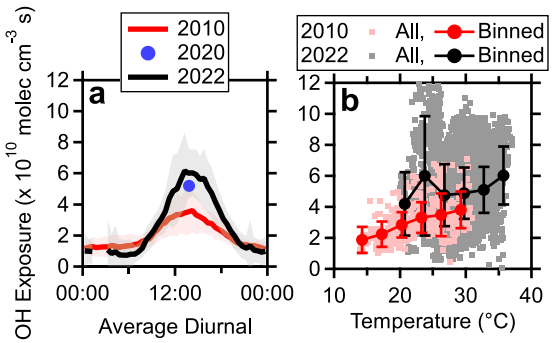


**Figure 2.** OH exposure average diurnals (a) and trends with temperature from during the day (b; 10:00–18:00 PDT) in 2010 (de Gouw et al., 2017) and 2022. The peak daytime OH exposure in 2020 was reported by Van Rooy et al. (2021). Diurnal averages (a) represent 30-min bins and shaded regions are one standard deviation. OH exposure in (b) was averaged by temperature bins (10–40°C; 3°C bins) where the error bars denote one standard deviation. For clarity, the average markers in (b) are offset from the center of the temperature bins. The 2022 data were averaged to 1 min.

$$[\mathrm{OH}]\Delta t = \frac{1}{k_{\mathrm{HC+OH}} - k_{\mathrm{Ben+OH}}} \times \left( \ln\left(\frac{\mathrm{Ben}}{\mathrm{HC}}\right) - \ln(\mathrm{ER}_{\mathrm{Ben/HC}}) \right) \quad (1)$$

Here, benzene (Ben) is used as the longer-lived reference for the more reactive hydrocarbon (HC). Benzene reacts with OH with a relatively slow rate coefficient ($k_{\mathrm{Ben+OH}}$) compared to that of the other hydrocarbon ($k_{\mathrm{HC+OH}}$). OH exposure is zero when their ratio equals their emission ratio ($ER_{\mathrm{Ben/HC}}$) and no losses have occurred. For this study, OH exposure was calculated using both C8 and C9 aromatics. Benzene and higher aromatics are used here to primarily assess oxidation of mobile source emissions. Although other emission sources for aromatics exist, such as VCPs (Stockwell et al., 2021), we assume mobile sources are still the dominant contributors to these hydrocarbons as evidenced by their correlation with CO. As mobile sources are ubiquitous, the derived OH exposure broadly reflects oxidation in the LA basin, in particular for emissions from other nonpoint sources. Additionally, air masses are continuously mixed, including those which were freshly emitted, as well as those with various degrees of aging. The reported OH exposure from these calculations represents the average exposure for air masses sampled at the site. By using similar hydrocarbons as other studies, the OH exposure estimated here can be quantitatively compared to previous studies at Caltech (de Gouw et al., 2017; Van Rooy et al., 2021).

Benzene-to-hydrocarbon emission ratios were estimated via regressions of the nighttime measurements with the assumption of negligible photochemical processing (Figure S6a in Supporting Information S1). This assumption does not apply for hydrocarbons that react efficiently with ozone or nitrate radicals, namely alkenes. This calculation also assumes benzene and the hydrocarbons come from the same or spatially coincident sources with a constant diurnal ratio. Here, mobile sources, which are ubiquitous in the LA basin, are assumed to be the dominant sources of aromatic hydrocarbons and the resulting OH exposure reflects the aging of related emissions. The $\mathrm{ER}_{\mathrm{Ben/C9\ Aromatics}}$ was determined to be 0.745 ± 0.008 ppbv ppbv$^{-1}$. From the GC-Vocus chromatograms, the relative abundance of 1,2,4-trimethylbenzene was ~56% of the C9 aromatics signal on average, and thus the 1,2,4-trimethylbenzene emission ratio was ~1.33 ppbv ppbv$^{-1}$, which is lower than those reported for CalNex-2010, 1.75 ± 0.15 ppbv ppbv$^{-1}$ (de Gouw et al., 2017), and LAAQC-2020, 1.84 ppbv ppbv$^{-1}$ (Van Rooy et al., 2021), both of which used GC measurements. However, the ambient ratio of benzene to C9 aromatics regularly falls to the emission ratio reported here, representing an upper limit (Fig. S6b in Supporting Information S1). During the 2022 measurements, consistent meteorology (warm and sunny) provided little diversity in measurement conditions. The lack of cooler, overcast days limits the ability to constrain these emission ratios using nights with negligible aging, likely resulting in *overestimations* of the benzene-hydrocarbon emission ratios.

OH exposure was calculated and averaged across C8 and C9 aromatics at each point in time (Figure S7 in Supporting Information S1). Figure 2 compares this average OH exposure to CalNex-2010 (de Gouw et al., 2017) and LAAQC-2020 (Van Rooy et al., 2021). It is worth noting that these two studies used 1,2,4-trimethylbenzene to derive OH exposure whereas this study used an average of all isomers of C8 and C9 aromatics. A weighted average rate coefficient was used for each group of isomers. However, these mixtures are expected to become less reactive as they age, likely leading to an underestimation at longer OH exposure. The average peak daytime OH exposure in 2020 and 2022 agree. The 2020 value is slightly lower, but this average represents measurements from April to July, whereas the measurements here spanned from July to August, and the warmer temperatures in late summer are expected to have more favorable conditions for photochemistry. Relative to the 2010 measurements, which spanned from May to June, daytime OH exposure was ~35% higher (statistically significant at 95% confidence) when comparing observations in the same temperature range of 25–30°C. The peak daytime OH exposure in 2022 was ~68% higher on average (statistically significant at 95% confidence) due to higher average ambient temperatures during the campaign. The benzene-hydrocarbon emission ratios for 2022, as discussed in the previous paragraph, are possibly overestimated. Reducing the emission ratios would shift the OH exposure curve up, thereby increasing the difference between 2022 and 2010.

OH exposure increased with temperature during the day (10:00–18:00 PDT; Figure 2b) following increased ozone production (Nussbaumer & Cohen, 2020; Pusede et al., 2015). Importantly, daytime OH exposure was higher in 2022 than 2010 in each temperature bin, suggesting faster photochemistry under assumed similar meteorological conditions The hydrocarbons' values of $k_{HC+OH}$ are expected to increase with temperature, ~1% in the case of benzene (Atkinson & Arey, 2003), contributing a negligible fraction to the enhanced average OH exposure. Histograms of ambient temperatures show similar distributions between the two years, except 2022 was shifted ~6.5°C on average toward warmer temperatures (Figure S8a in Supporting Information S1), which contributed to a shift toward higher OH exposure (Figure S8b in Supporting Information S1). OH exposure in 2022 was lower in the cooler temperature range, typically associated with nighttime (Figure S5 in Supporting Information S1) as seen in the average diurnal (Figure 2a). In short, the 2022 measurements experienced faster photochemistry due to, in part, reduced cloud coverage (as demonstrated in Figure S4 in Supporting Information S1), higher average daytime temperatures, and other factors that correlate with temperature. A different $NO_x$-VOC chemical regime may also contribute to faster photochemistry, which is discussed further in the context of ozone concentrations in Section 3.4.

### 3.3. Emission Ratios of Precursors

Hydrocarbon emission ratios relative to CO were estimated using methods similar to those presented in the literature (Borbon et al., 2013; de Gouw et al., 2017; Roberts et al., 1984). Specifically, the emission ratios are relative to the enhancements in CO above the atmospheric background concentration ($CO_{bkg}$), ΔCO. $CO_{bkg}$ was determined from linear regressions of reactive hydrocarbons with CO using nighttime data only. Extrapolation to zero hydrocarbon concentration is assumed to represent the regional CO background concentration with minimal influence from local emissions. This estimation assumes that $CO_{bkg}$ is constant during the measurement period. Additionally, this estimation requires reactive hydrocarbons that themselves do not have a regional background concentration, otherwise this calculation can underestimate $CO_{bkg}$ (de Gouw et al., 2017). Here, the estimated $CO_{bkg}$ was derived as the average (and standard deviation) of the extrapolated values using C8 and C9 aromatics (Fig. S9 in Supporting Information S1). In this study, the $CO_{bkg}$ is estimated to be 112 ± 3 ppbv which is similar to the value of 115 ± 10 ppbv reported from CalNex-2010 (de Gouw et al., 2017). During LAAQC-2020, $CO_{bkg}$ was reported as 90 ± 15 ppbv (Van Rooy et al., 2021). The LAAQC-2020 measurements were made in response to the COVID-19 shelter-in-place restrictions. During this time, human activity was significantly reduced, impacting corresponding emissions. Reductions in local, regional, and global traffic counts may have contributed to a reduced $CO_{bkg}$. On the other hand, decreases in global CO backgrounds since 2010 have been significant due to reduced global emissions from transportation, industry, and biomass burning (Buchholz et al., 2021; Zheng et al., 2019). The estimation of $CO_{bkg}$ in this work is limited due to the use of only C8 and C9 aromatics. If the true $CO_{bkg}$ has declined since the 2010 measurements, then the hydrocarbon emission ratios relative to CO estimated in this study would be overestimated.

Hydrocarbon emission ratios relative to CO ($ER_{HC}$) were derived by a multivariate regression involving measured hydrocarbon mixing ratios, enhancements in CO (ΔCO), and OH exposure (Fig. S10 in Supporting Information S1). The measured mixing ratios (HC) can be described according to Equation 2:

$$HC = HC_{bkg} + ER_{HC} \times \Delta CO \times e^{-(k_{HC+OH} - k_{CO+OH})[OH]\Delta t} \quad (2)$$

where $HC_{bkg}$ is the atmospheric background concentration of the hydrocarbon. The rate coefficient of CO with OH, $k_{CO+OH}$, was taken from Atkinson and Arey (2003). More reactive compounds ($k_{HC+OH} \geq 5 \times 10^{-12}$ $cm^3$ $molec^{-1}$ $s^{-1}$) were assumed to have a negligible $HC_{bkg}$, so $HC_{bkg}$ was set to 0 pptv. Average fitting parameters and uncertainties were determined by doing the same calculation with high and low (±1 standard deviation) $\Delta CO$ and OH exposure and taking the standard deviation of the results. Benzene was insensitive to uncertainties in OH exposure due to its slow reaction rate.

Table 1 summarizes the emission ratios calculated in this study and Figure 3 compares emission ratios of some aromatics against previous studies. The uncertainties in the reported emission ratios reflect the uncertainties in the multivariate regressions using Equation 2, but are likely greater due to measurement uncertainties (estimated as ±10% for the standards in Tables S1 and S2 in Supporting Information S1, excluding acetaldehyde and isoprene due to the corrections, and ±50% for everything else). Relative to 2010, benzene, toluene, C8 aromatics, and C9

**Table 1**
*Hydrocarbon, Oxygenated VOC (OVOC), and VCP Emission Ratios (ER)*

| | Species | $k_{VOC+OH}$ ($10^{-12}$ cm$^3$ molec$^{-1}$ s$^{-1}$) | ER ± ΔER (pptv [ppbv CO]$^{-1}$) | | | $r^2$ |
|---|---|---|---|---|---|---|
| | | | 2022, this work | 2020[p] | 2010[o] | 2022 |
| Hydrocarbons | Benzene | 1.22[a] | 0.9218 ± 0.0005 (±10%) | 0.64 ± 0.17 | 1.260 ± 0.011 | 0.43 |
| | Toluene | 5.63[a] | 3.18 ± 0.10 (±10%) | 2.84 ± 0.38 | 3.40 ± 0.17 | 0.77 |
| | C8 Aromatics | 16.4[a,b] | 3.2 ± 0.2 (±10%) | 2.22 ± 0.2 | 3.5 ± 0.2 | 0.88 |
| | C9 Aromatics | 32.4[a,b] | 1.52 ± 0.09 (±10%) | 1.29 ± 0.09 | 2.17 ± 0.10 | 0.85 |
| | C10 Aromatics | 55.5[c,d] | 0.56 ± 0.04 (±50%) | | | 0.81 |
| | C11 Aromatics | 103[c,d] | 0.108 ± 0.005 (±50%) | | | 0.59 |
| | C12 Aromatics | 113[a,d] | 0.0334 ± 0.0007 (±50%) | | | 0.17 |
| | Naphthalene | 23[a] | 0.138 ± 0.010 (±50%) | | | 0.15 |
| | Methylnaphthalene | 44.8[e,f] | 0.088 ± 0.008 (±50%) | | | 0.54 |
| | Acenaphthene | 80[g] | 0.008 ± 0.003 (±50%) | | | 0.10 |
| | Dimethylnaphthalene | 64.3[d,f] | 0.036 ± 0.004 (±50%) | | | 0.50 |
| | Fluorene | 16[h] | 0.0041 ± 0.0009 (±50%) | | | 0.19 |
| Oxygenated VOCs | Methanol | 0.94[a] | 27.7 ± 0.2 (±10%) | | 21.2 ± 1.4 | 0.54 |
| | Ethanol | 3.2[a] | 185 ± 8 (±10%) | | 45.7 ± 1.0 | 0.75 |
| | Formic Acid | 0.45[i] | 0.752 ± 0.006 (±50%) | | 1.2 ± 0.8 | 0.47 |
| | Acetic Acid | 0.8[i] | 14.91 ± 0.03 (±50%) | | | 0.65 |
| | Acetaldehyde | 15[a] | 10.4 ± 0.3 (±10%) | | 4.3 ± 0.8 | 0.66 |
| | Acrolein | 19.6[j] | 1.65 ± 0.04 (±10%) | | 1.40 ± 0.03 | 0.75 |
| | Acetone | 0.17[a] | 16.2 ± 0.8 (±10%) | | 11.6 ± 1.1 | 0.65 |
| | C4 Carbonyls | 1.22[a,k] | 1.92 ± 0.02 (±10%) | | 1.3 ± 0.2 | 0.67 |
| | C6 Carbonyls | 9.1[a,k] | 0.355 ± 0.014 (±10%) | | | 0.71 |
| | C7 Carbonyls | 11[a,k] | 0.449 ± 0.009 (±50%) | | | 0.69 |
| | C8 Carbonyls | 11[a,k] | 0.282 ± 0.006 (±50%) | | | 0.58 |
| | C9 Carbonyls | 12[a,k] | 0.290 ± 0.011 (±50%) | | | 0.60 |
| | C10 Carbonyls | 12[a,k] | 0.094 ± 0.002 (±50%) | | | 0.37 |
| Volatile Chemical Products | Decamethyltetrasiloxane (L4) | 2.5[l] | 0.0021 ± 0.0002 (±50%) | | | 0.44 |
| | Dodecamethylpentasiloxane (L5) | 3.4[l] | 0.00163 ± 0.00003 (±50%) | | | 0.44 |
| | Hexamethylcyclotrisiloxane (D3) | 0.86[l] | 0.01598 ± 0.00005 (±10%) | | | 0.42 |
| | Octamethylcyclotetrasiloxane (D4) | 1.3[l] | 0.0332 ± 0.0002 (±10%) | | | 0.17 |
| | Decamethylcyclopentasiloxane (D5) | 2.1[l] | 0.239 ± 0.002 (±10%) | | | 0.06 |
| | Dichlorobenzene | 0.49[f,m] | 0.0936 ± 0.0002 (±50%) | | | 0.29 |
| | *para*-Chlorobenzotrifluoride (PCBTF) | 0.23[n] | 0.40532 ± 0.00003 (±50%) | | | 0.26 |

*Note*. Error bars (ΔER) reflect the uncertainty from the multivariate fits. The measurement uncertainties are provided in parentheses and are more representative of the emission ratio uncertainties. The correlation coefficient, $r^2$, corresponds to the correlation between the measured time series in 2022 and the 2022 time series reconstructed using the multivariate fits described in Equations 2 and 3 as well as the derived parameters. [a](Atkinson & Arey, 2003). [b]Average of isomers weighted by the average relative abundance in GC-Vocus chromatograms. [c](Aschmann et al., 2013). [d]Rate coefficient of the methyl-substituted benzenes only. [e](Phousongphouang & Arey, 2002). [f]Unweighted average of isomers. [g](Reisen & Arey, 2002). [h](Kwok et al., 1997). [i](Atkinson et al., 1997). [j](Atkinson, 1986). [k]Rate coefficient of the 2-ketone only. [l](Alton & Browne, 2020). [m](Wahner & Zetzsch, 1983). [n](Atkinson et al., 1985). [o](de Gouw et al., 2017, 2018). [p](Van Rooy et al., 2021).

aromatics experienced ~26%, ~6%, ~9%, and ~30% reductions in emission ratios, respectively. Emissions of CO and these aromatic hydrocarbons appear to have decreased together between 2010 and 2022, resulting in similar emission ratios but lower overall concentrations. These observations suggest that mobile sources were still the primary emitters of these species and the average emission control system efficiency of the fleet has improved over the 12 years between studies. Differences between the aromatics' emission ratio reductions potentially point toward a shift in mobile versus VCP contributions. For example, Stockwell et al. (2021) identified emissions of aromatics from solvent-borne coatings, but found minor emissions of benzene compared to toluene and larger

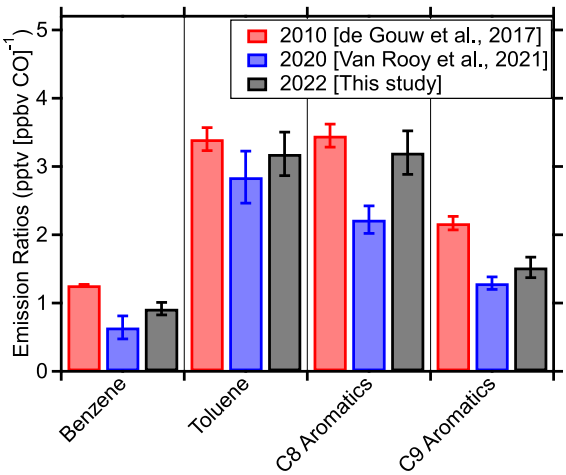


**Figure 3.** Emission ratios relative to CO and corrected for OH exposure for 4 aromatic hydrocarbons.

aromatics. The ~26%–30% reduction in benzene and C9 aromatics emission ratios may be more representative of changes in mobile source emissions. Weaker reductions in toluene and C8 aromatics emission ratios may reflect negligible reductions in VCP emissions or perhaps enhanced emissions, which offset reduced mobile source emissions, due to higher temperatures and evaporation rates. The toluene and C9 aromatics emission ratios agree with the values from 2020, but the benzene and C8 aromatics emission ratios were higher. These differences may reflect different emission compositions between the COVID-19 shelter-in-place period and business-as-usual. Additionally, Equation 2 was used to reconstruct the hydrocarbon time series using these average fitting parameters, CO, and OH exposure for comparisons against the measured time series. The reconstructed time series generally captured long-term variability, and the correlations ($r^2$; Table 1) between the reconstructed and measured time series were generally good with a few exceptions discussed below.

Higher instrument sensitivity and lower limits of detection have allowed for the determination of emission ratios for more precursors, including C10–C12 aromatics and polycyclic aromatic hydrocarbons (PAHs), which were not quantified during CalNex-2010 (Table 1). Semivolatile and intermediate volatility organic compounds (SVOCs and IVOCs, respectively) are known to have significant contributions to the formation of SOA (Dzepina et al., 2009; de Gouw et al., 2011; Khare et al., 2020; R. Li et al., 2013; Liggio et al., 2016; Robinson et al., 2007). These precursors are often missing or underreported in studies of ambient air due to instrumentation limitations. The emission ratios reported here may help to constrain SOA formation. It should be noted that, while the multivariate fits captured the broad characteristics of the measurements, the correlation coefficients ($r^2$) between the measured concentrations and recreated time series for some of these species are low. For VOCs with low mixing ratios, the linear correlation may be limited by the statistical noise in the measurements. PAHs have additional, temperature-dependent evaporative sources such as asphalt-related materials that are not correlated with mobile source emissions (Khare et al., 2020). In addition, the poor correlations for some VOCs are primarily driven by brief high-concentration emissions, which were not captured in the fits (Fig. S11 in Supporting Information S1).

### 3.4. Ambient Concentrations of Oxygenated VOCs

Oxygenated VOCs (OVOCs) have many emission sources related to mobile sources (Clairotte et al., 2013; P. Liu et al., 2024), biomass burning (Gilman et al., 2015; Koss et al., 2018), cooking (Coggon, Stockwell, Xu, et al., 2024; Klein et al., 2016; Schauer et al., 1999), and VCPs (G. Liu et al., 2024; S. Wang et al., 2024), as well as secondary sources from photochemical production from the oxidation of precursors. These OVOCs can then undergo oxidation themselves and/or, as in the case of carbonyls, undergo photolysis during the day (Griffith et al., 2016). Figure 4 shows the average diurnals and temperature dependence of ozone and a few OVOCs.

Average ozone concentrations were generally comparable between 2010 and 2022 (Figure 4a). The peak daytime ozone concentration was ~20% higher in 2022 than 2010, but average daytime concentrations were lower in 2022 for each temperature bin (Figure 4f). Only daytime data are compared in Figure 4f to focus on daytime photochemical production of ozone. Similar observations are made if only afternoon data (14:00–16:00 PDT) are compared. Despite increasing temperatures, which appear to have caused increased oxidation and faster ozone formation, similar overall ozone concentrations suggest that other processes have impacted ozone between 2010 and 2022. One possibility is that $NO_x$ reductions are resulting in a gradual transition in ozone production regimes as previous studies have suggested (Kim et al., 2022; Nussbaumer & Cohen, 2020; Schroeder et al., 2022; Zhu et al., 2022). Further reductions in $NO_x$ and VOC emissions may lead to further reductions of ozone, but the frequency of droughts and heat waves in California are expected to increase with the changing climate (Swain et al., 2014). However, further investigations are necessary to fully understand the current chemical regime of the LA basin. Here, temperature is used as a proxy for other factors such as solar irradiance, atmospheric stagnation, and other meteorological conditions, which are favorable to ozone formation. There are obviously more factors that influence ozone production, but a detailed study of ozone trends is not the focus of this study.

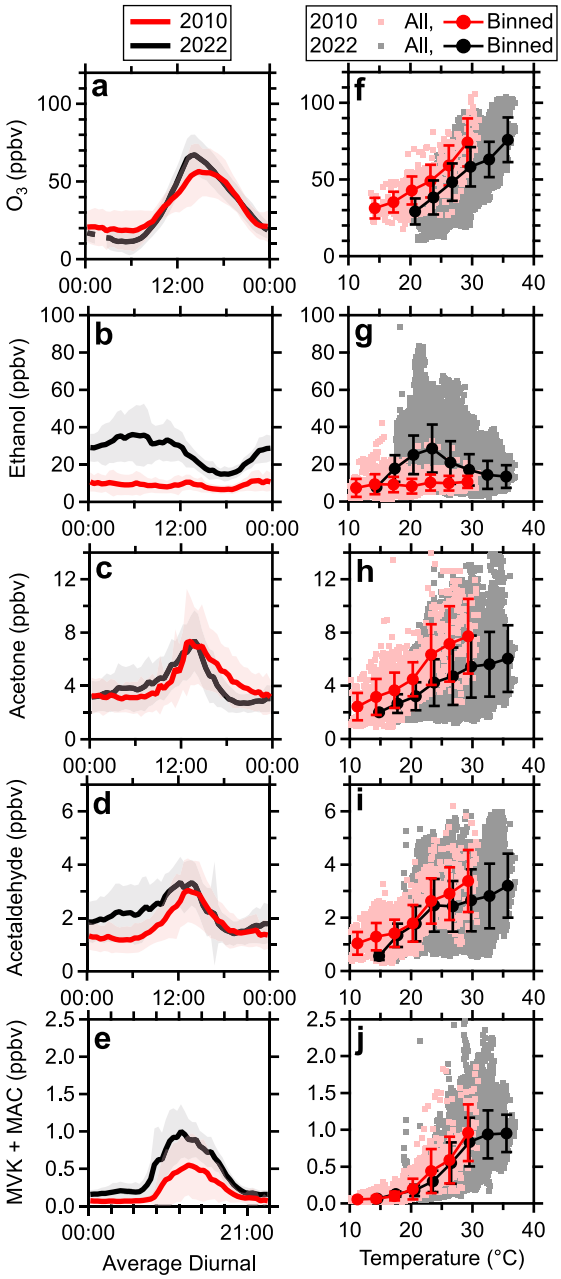


**Figure 4.** Mixing ratio diurnal averages (a–e) and mixing ratio trends with temperature during the day for ozone (f; 10:00–18:00 PDT) and all times of day for selected OVOCs (g–j) in 2010 and 2022. Diurnal averages (a–e) represent 30-min bins and shaded regions are one standard deviation. Mixing ratios in (f–j) were averaged by temperature bins (10–40°C; 3°C bins) where the error bars denote one standard deviation. For clarity, the average markers in (f–j) are offset from the center of the temperature bins. The 2022 mixing ratios are averaged to 1 min.

The differences in concentrations of OVOCs between 2010 and 2022 varied according to the respective sources. Ethanol, which is mostly a primary emission from VCPs and its use as a gasoline additive, generally had higher concentrations in 2022. Emission control strategies have primarily targeted vehicle exhaust while VCP emissions have remained largely unregulated. More oxygenated formulations of VCPs are also becoming more common, as in the case of paints (Stockwell et al., 2021). Higher temperatures may have also contributed to enhanced evaporative emissions from VCPs, fuels, asphalt, and other sources (Cao et al., 2023; Khare et al., 2020; Wu et al., 2024). During the day, ethanol is removed rather than produced as evidenced by the midday reduction in its diurnal (Figure 4b) and reduced concentrations at higher temperatures (Figure 4g) due to higher OH exposures (Figure 2b) as discussed further in Section 3.7. Data from all times of day are used to investigate the OVOCs' temperature dependences (Figures 4g–4j) as they have both primary and secondary sources. Using airborne flux measurements, Pfannerstill et al. (2024) observed increasing ethanol (and other VOC) emissions with increasing temperatures in Los Angeles. In combination with the measurements presented here, ethanol mixing ratios, and possibly those of other VOCs, may be more controlled by loss processes at higher temperatures compared to emissions. For ethanol, the transition temperature where loss processes appear to take over occurs at ~23.5°C.

Acetone and acetaldehyde share similar diurnal profiles and magnitudes between 2010 and 2022 (Figures 4c and 4d). Both show afternoon enhancements, which are indicative of photochemical production and, possibly, daytime emissions. As with ozone, the concentrations in each temperature bin were lower in 2022 (or comparable in the case of lower temperature bins for acetaldehyde; Figures 4h and 4i), which indicates slower production and/or lower emissions at a given temperature, but similar overall concentrations due to warmer temperatures.

Methyl vinyl ketone (MVK) and methacrolein (MAC) are mostly produced from isoprene OH oxidation and show strong daytime enhancements in both 2010 and 2022 (Figure 4e). With similar average isoprene concentrations relative to 2010 (Figure 1e), MVK and MAC (and crotonaldehyde) had nearly double the average daytime maximum concentration. For each temperature bin, isoprene concentrations were generally lower (Figure 1j), although the 2010 measurements may be less representative as discussed in Section 3.1. However, MVK and MAC concentrations were generally equivalent in each bin (Figure 4j). Emissions of MVK's and MAC's precursor, isoprene, decline at temperatures above 37°C (Z. Li et al., 2011; Rasulov et al., 2010), which appears to occur at the highest temperatures in Figure 1j as isoprene seems to approach a maximum concentration. The elevated nighttime concentrations of MVK and MAC may stem from residual daytime production or from a contribution of crotonaldehyde from cooking to this molecular formula (Schauer et al., 1999).

At any given temperature, secondary production appears comparable or lower for these species compared to 2010. As with ozone, the higher average temperatures in 2022 seem to have offset any reductions such that average concentrations were comparable to those in 2010. However, these differences in OVOC concentrations may also involve changes in primary emissions.

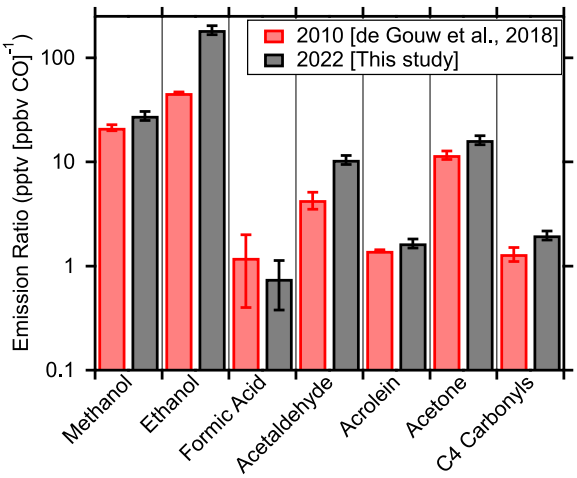


**Figure 5.** Emission ratios of OVOCs relative to CO and corrected for OH exposure.

### 3.5. Primary Emissions and Secondary Production of OVOCs

To investigate the relative contributions of primary emissions and secondary formation of OVOCs, we adopt the framework set forth by de Gouw et al. (2018), in which the measured time series for each OVOC is fit by the following equation:

$$\mathrm{OVOC} = \mathrm{OVOC_{bkg}} + \mathrm{ER_{OVOC}} \times \Delta\mathrm{CO} \times e^{-(k^*_{\mathrm{OVOC}} - k_{\mathrm{CO+OH}})[\mathrm{OH}]\Delta t} + \mathrm{ER_{Prec}} \times \Delta\mathrm{CO} \times \frac{k_{\mathrm{Prec+OH}}}{k^*_{\mathrm{OVOC}} - k_{\mathrm{Prec+OH}}} \times \left(e^{-(k_{\mathrm{Prec+OH}} - k_{\mathrm{CO+OH}})[\mathrm{OH}]\Delta t} - e^{-(k^*_{\mathrm{OVOC}} - k_{\mathrm{CO+OH}})[\mathrm{OH}]\Delta t}\right) \quad (3)$$

In Equation 3, the measured mixing ratio (OVOC) is a function of the atmospheric background concentration ($\mathrm{OVOC_{Bkg}}$; term 1) and the emission ratio relative to CO ($\mathrm{ER_{OVOC}}$), accounting for primary emission of the OVOC (term 2) as in Equation 2. This primary emission term assumes a correlation with CO. Although this assumption may apply for some OVOC emissions, for example, from mobile sources (Clairotte et al., 2013; P. Liu et al., 2024), many OVOCs are not expected to be co-emitted with CO. Here, CO serves as a proxy for general human activity, but there is likely greater uncertainty in the derived emission ratios for species with different emission diurnals. A third term accounts for secondary production and removal via the emission of precursors including the weighted average emission ratio relative to CO ($\mathrm{ER_{Prec}}$) and rate coefficient ($k_{\mathrm{Prec+OH}}$) of all precursors. These parameters, as well as $\mathrm{OVOC_{bkg}}$ and $\mathrm{ER_{OVOC}}$, are freely fit in the multivariate regression; only the effective loss rate coefficient ($k^*_{\mathrm{OVOC}}$) is held constant. This effective loss rate coefficient represents a combination of the loss rate to OH and photolysis (where photolysis is assumed to scale with OH concentration), as detailed in Text S1 in Supporting Information S1 and described by de Gouw et al. (2018). As with determining precursor emission ratios in Section 3.3, the fit was repeated with high and low ΔCO and OH exposure to determine uncertainties and average fitting parameters.

Table 1 and Figure 5 summarize the primary emission ratios from the multivariate fits and compare them to 2010. Emission ratios of OVOCs were generally higher in 2022. Formic acid had an approximately equivalent emission ratio between the two studies. These higher emission ratios possibly follow from reduced CO emissions from vehicle sources and unregulated VCP emissions. Increased evaporative emissions with higher temperatures and the sampling location may also play a role in enhancing emission ratios. Determination of emissions ratios relies significantly on the nighttime data when OH exposure is low. Equation 3 does not account for nighttime formation of OVOCs from the reactions of alkenes with ozone and nitrate radicals, which have been observed in the LA basin (de Gouw et al., 2017) to form aldehydes and acids. These nighttime reactions may cause overestimates of the emission ratios reported here.

Figure 6 shows the enhancement ratios relative to CO for ethanol, acetone, acetaldehyde, and formic acid as a function of OH exposure with the multivariate fit of Equation 3 with the data in the left column. The right column shows the average diurnal variation of the measurements as well as the reconstruction using the three terms from the fit: atmospheric background, primary emissions, and secondary formation.

Ethanol concentrations persist into the late morning, possibly due to strong primary emissions from rush hour traffic as well as increasing evaporative emissions as temperatures rise. In the early afternoon, at peak OH exposure, ethanol concentrations decline due to oxidation to acetaldehyde. The multivariate fit captured this behavior and assigned no secondary formation of ethanol. The missing contribution to ethanol in the early morning (~6 a.m.) may represent a source not correlated with CO emissions. Moreover, the overestimation of daytime concentrations may be caused by the assumption that ethanol is co-emitted with CO when other sources play an important role.

Acetone, acetaldehyde, and formic acid all have primary and secondary contributions to their ambient concentrations. Contributions from primary emissions occurred throughout the day, dipping in the afternoons, and secondary contributions were negligible at night, peaking at midday. At noon, primary and secondary contributions were split approximately evenly for each species. Analyses of the 2010 data yielded a similar distribution

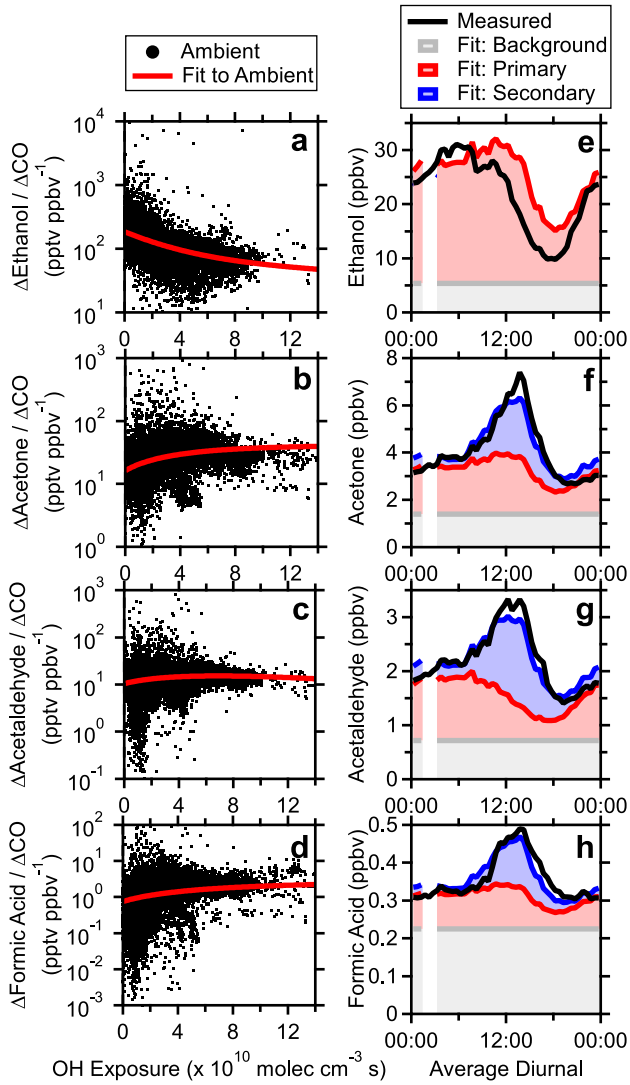


**Figure 6.** Multivariate fits (Equation 3) of selected OVOCs (a–d) and the corresponding diurnal averages of the atmospheric background, primary emissions, and secondary formation contributions (e–h).

of primary and secondary contributions for acetone, but much smaller contributions from primary emissions of acetaldehyde and formic acid, less than one-third and one-tenth of the daytime concentrations, respectively (de Gouw et al., 2018). Therefore, the relative contributions of primary emissions and secondary formation seem to have shifted in favor of primary emissions since 2010. Secondary production appeared to be approaching its limit with increasing OH exposure (as discussed in the next paragraph), while primary emissions have increased with unregulated VCP use and likely greater evaporation associated with higher temperatures. Since OH exposure may have been underestimated as discussed in Section 3.2, the distribution between primary and secondary contributions in this study would shift toward more secondary formation if a higher OH exposure was used. Even so, as temperatures increase in LA, we expect to see more primary emissions.

The secondary production of acetone, formic acid, and acetaldehyde via oxidation proceeded as expected. Both acetone and formic acid continued to form as the OH exposure increased (Figures 6b and 6d). They both react relatively slowly with OH, so the high OH exposure contributed to net formation for these measurements. However, the multivariate fits approach an asymptote; production appears to reach a limit at very high OH exposures as the relevant precursors fully react. Acetaldehyde reacts with OH nearly 100 times faster than acetone (Atkinson & Arey, 2003). At higher OH exposures, acetaldehyde begins to oxidize faster than it is formed from precursors, leading to a turn-over in ambient concentrations and the multivariate fit (Figure 6c).

In combination, our results show that concentrations of primary hydrocarbons and CO have declined from 2010 to 2022 due to reduced emissions, whereas concentrations of OVOCs and ozone have changed little. Emission ratios of primary OVOCs have increased, in part, due to reduced CO emissions from vehicles and possibly enhanced evaporative emissions given higher temperatures. Higher OH exposure is evidence of faster photochemistry, contributing to the formation and oxidation of OVOCs.

### 3.6. Day-To-Night Ratios of Precursors and OVOCs

To explore the full information contained in the Vocus measurements about emissions and chemical transformations, the day- and nighttime averages of all measured signals for the full measurement period were grouped by elemental composition and summed. The total daytime signal was ~11% higher than that of the nighttime (Figure 7). This average difference encompasses the changes for each family. Hydrocarbons ($C_xH_y$) were ~24% lower during the day than at night. Single-oxygen species ($C_xH_yO$) were enhanced by ~26%. The greatest contribution to this family was from acetone, which was enhanced ~64%. OVOCs with multiple oxygen atoms ($C_xH_yO_2$ and $C_xH_yO_{\geq 3}$) also demonstrated daytime enhancements, while all other families generally had higher nighttime concentrations. To account for varying instrument response and sensitivities, signals (in counts per second; cps) were normalized (in normalized cps; ncps) to the time-varying average sensitivity. It should be noted that different functional groups have different proton-transfer reaction rate coefficients, so different families should only be compared semi-quantitatively. Family compositions may vary between day and night, so comparisons of the same families between day and night should be made cautiously. With this in mind, the day-to-night ratios were calculated for each molecular formula.

Figure 8 summarizes the day-to-night ratios of all measured species (sorted by highest to lowest ratio, the "ratio index") and the different families are plotted separately. These ratios compare normalized count rates and are therefore independent of sensitivities. A possible exception occurs when different isomers contribute to a signal during day and night. These ratios for each VOC and trends across families help to elucidate their sources and fates. Ratios of <1 indicate daytime losses and sources related mostly to primary emissions. Ratios of ~1 mean

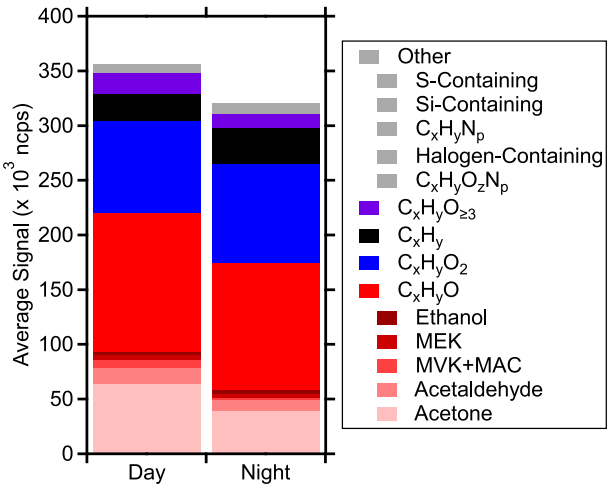


**Figure 7.** Normalized signals (ncps; stacked bars) during day and night averaged across the field measurements. The 582 identified ions are grouped by elemental composition. Selected signals in the $C_xH_yO$ family are shown separately due to their significant contributions to the total signal. Day and night comparisons for each ion are shown in Figure 8.

that day and night concentrations are comparable. Dilution and photochemical losses during the day must be offset by daytime emissions and/or photochemical production. Ratios >1 suggest photochemical production and/or only daytime emissions.

Hydrocarbons all had ratios of <1 except for isoprene, the emissions of which are light-dependent (Sanadze, 2004), and $C_{18}H_{36}H^+$, which had a low signal contributing to an uncertain ratio (Figure 8a). Monoterpenes (MTs) and sesquiterpenes (SQTs) have day- and nighttime biogenic emissions, albeit with a lower magnitude at night. Due to slower nighttime oxidation and lower boundary layers, nighttime monoterpene ratios are commonly higher than during the day. MTs also have strong anthropogenic emissions from VCPs (Gkatzelis, Coggon, McDonald, Peischl, Aikin, et al., 2021). Because of the combination of emission sources, chemistry, and dynamics, MTs have a day-to-night ratio of ∼1. Aromatics react with OH at different rates, which is reflected in their ratios: benzene reacts slowly and has a ratio of ∼1, while C8 and C9 aromatics have gradually higher rate coefficients with OH and declining ratios in turn. Toluene's ratio was similar to that of benzene, possibly due to significant daytime VCP emissions.

OVOCs had ratios ranging from ∼4 to ∼0.1 (Figure 8b). MVK and MAC had one of the highest ratios due to the daytime abundance of their precursor: isoprene. OVOCs with more oxygen atoms tended to have the highest ratios in general due to photochemical production as the main source whereas other OVOCs with fewer oxygen atoms also have primary emission sources, such as acetone, or only primary emission sources, such as ethanol. There is also evidence of MT oxidation products ($C_{10}H_{16}O_2H^+$ and $C_{10}H_{16}O_3H^+$), although their day-to-night ratios vary as they are formed by different chemistries: nitrate radicals serve as a nighttime oxidant (Day et al., 2022; DeVault et al., 2022; Jenks et al., 2023) while OH and to a lesser extent ozone are mostly daytime oxidants (Hantschke et al., 2021; Thomsen et al., 2022).

More isoprene and MT oxidation products containing nitrogen from reactions with NO, $NO_2$, and nitrate radicals were also observed (Figure 8c). Again, their ratios show a large range due to formation by different chemistries. Most reduced nitrogen-containing compounds had ratios below 1 as they only have primary sources such as VCPs, solvent use on Caltech campus, or biomass burning (Coggon et al., 2016; Koss et al., 2018; Sekimoto et al., 2018). Some of these species have ratios of ∼1, suggesting slow chemical removal or daytime emissions, possibly from evaporation.

Other compounds highlighted include organosulfur compounds and halogenated compounds. Dimethyl sulfide had a ratio of ∼1, likely due to significant marine biogenic emissions (Carpenter et al., 2012). Chloramine has a short photolysis lifetime estimated as several minutes (C. Wang et al., 2023), yielding a low day-to-night ratio. Chloramine photolysis acts as a source of chlorine radicals during the day, allowing for the formation of chlorinated products such as chloroacetone, which was observed here with an elevated day-to-night ratio and in Toronto during summer and winter (C. Wang et al., 2023). *Para*-Chlorobenzotrifluoride (PCBTF) is associated with solvent-based coatings and tended to have higher concentrations during the day (Figure 8d), likely due to strong daytime evaporation with high temperatures and generally more daytime use of the corresponding VCPs (Gkatzelis, Coggon, McDonald, Peischl, Aikin, et al., 2021; McDonald et al., 2018) as well as a slow reaction rate with OH (Chattopadhyay et al., 2022).

Some silicon-containing compounds are uniquely associated with VCPs: octamethylcyclotetrasiloxane (D4 siloxane) and decamethylcyclopentasiloxane (D5 siloxane) (Gkatzelis, Coggon, McDonald, Peischl, Aikin, et al., 2021; McDonald et al., 2018). D4 siloxane, associated with adhesives and insecticides, had a ratio of ∼1 for similar reasoning as PCBTF, including a slow reaction rate with OH (Alton & Browne, 2020). D5 siloxane is emitted from personal care products and had higher nighttime concentrations. Emission ratios relative to CO were estimated for these siloxanes using Equation 2 (Table 1) and will help to constrain VCP emissions. Although siloxanes are not emitted from combustion sources such as CO, they typically scale with population density alongside vehicle emissions (Gkatzelis, Coggon, McDonald, Peischl, Aikin, et al., 2021; Gkatzelis, Coggon, McDonald, Peischl, Gilman, et al., 2021). The reconstructed time series from the multivariate fits correlated

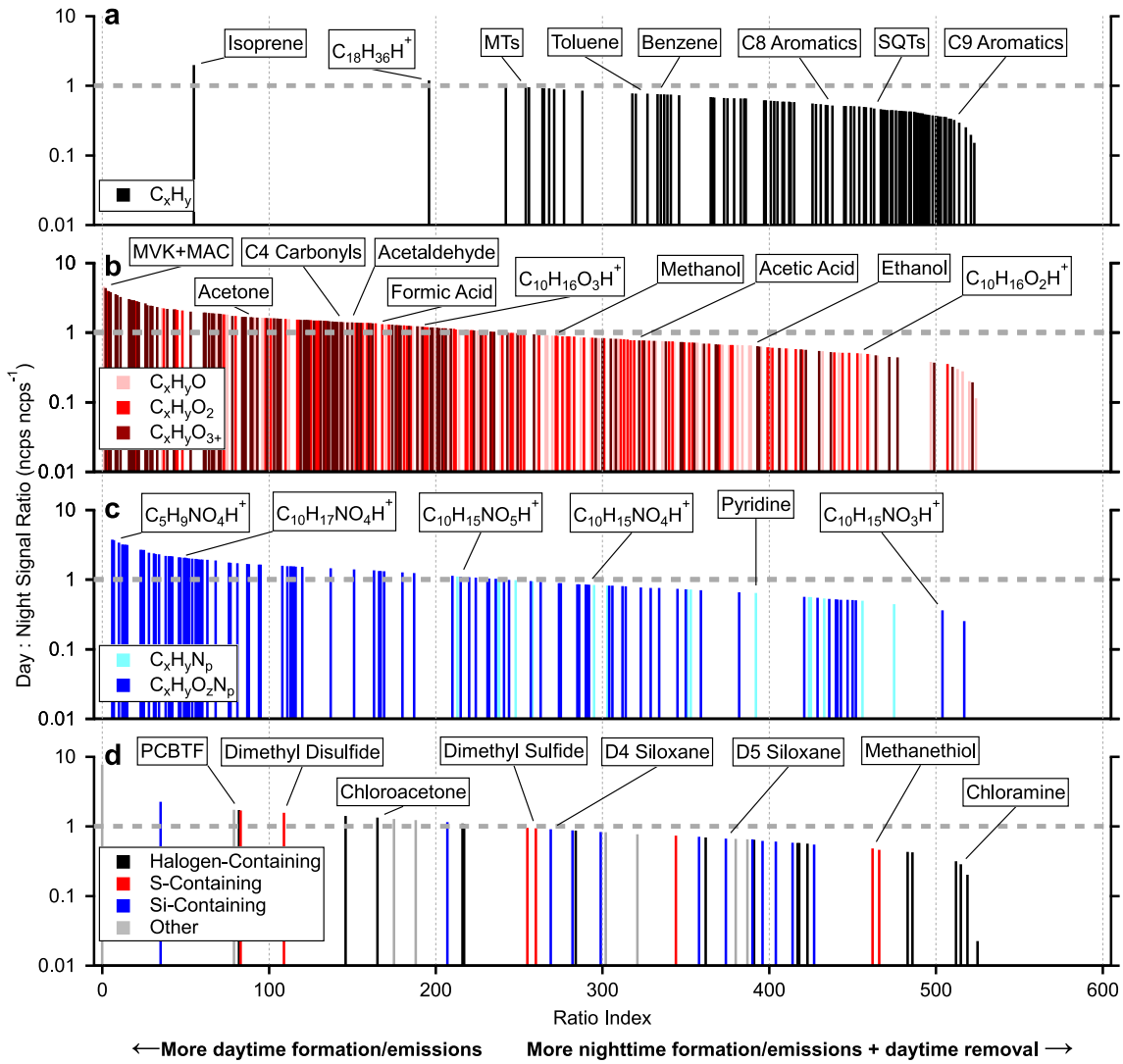


**Figure 8.** Average day-to-night ratios of the 582 identified ions, grouped into hydrocarbons (a), OVOCs (b), nitrogen-containing (c), and others (d). The ratio index is the order of VOCs sorted by highest ratio.

poorly ($r^2$ = 0.06) with the measurements for similar reasons as discussed with PAHs in Section 3.3; the multivariate fits captured the broad structures, but they failed to capture the frequent, fine structures (Fig. S12 in Supporting Information S1). Local emissions were common, particularly for D5 siloxane in the early morning when students, staff, and faculty arrived at the campus.

### 3.7. Insights From OFR Experiments

OFR-Vocus measurements were made to investigate the oxidation of precursors and formation of OVOCs and secondary organic aerosol in ambient air. OFR-Vocus measurements of C8 and C9 aromatics, acetone, and acetaldehyde are summarized in Figure 9. OH exposure in the OFR was estimated using hydrocarbon ratios in the same manner as ambient OH exposure (Section 3.2). Ambient daytime peak OH exposure was ~$6 \times 10^{10}$ molec cm$^{-3}$ s (campaign average of $2 \pm 2 \times 10^{10}$ molec cm$^{-3}$ s) and the average in OH exposure in the OFR (including contributions from ambient exposure) was ~$9 \times 10^{10}$ molec cm$^{-3}$ s (Figure 9a). The OFR enhanced OH exposure by $7 \pm 4 \times 10^{10}$ molec cm$^{-3}$ s above ambient exposure. Assuming an average 24-hr OH concentration of ~$1.5 \times 10^6$ molec cm$^{-3}$ (Mao et al., 2009), the midday photochemical age of ambient air was ~0.5 days, whereas the photochemical age downstream of the OFR ranged from ~0.5 to 1 day. The OFR-Vocus data therefore provide insights into current, natural oxidation processes, as well as predicts the chemistry of higher OH

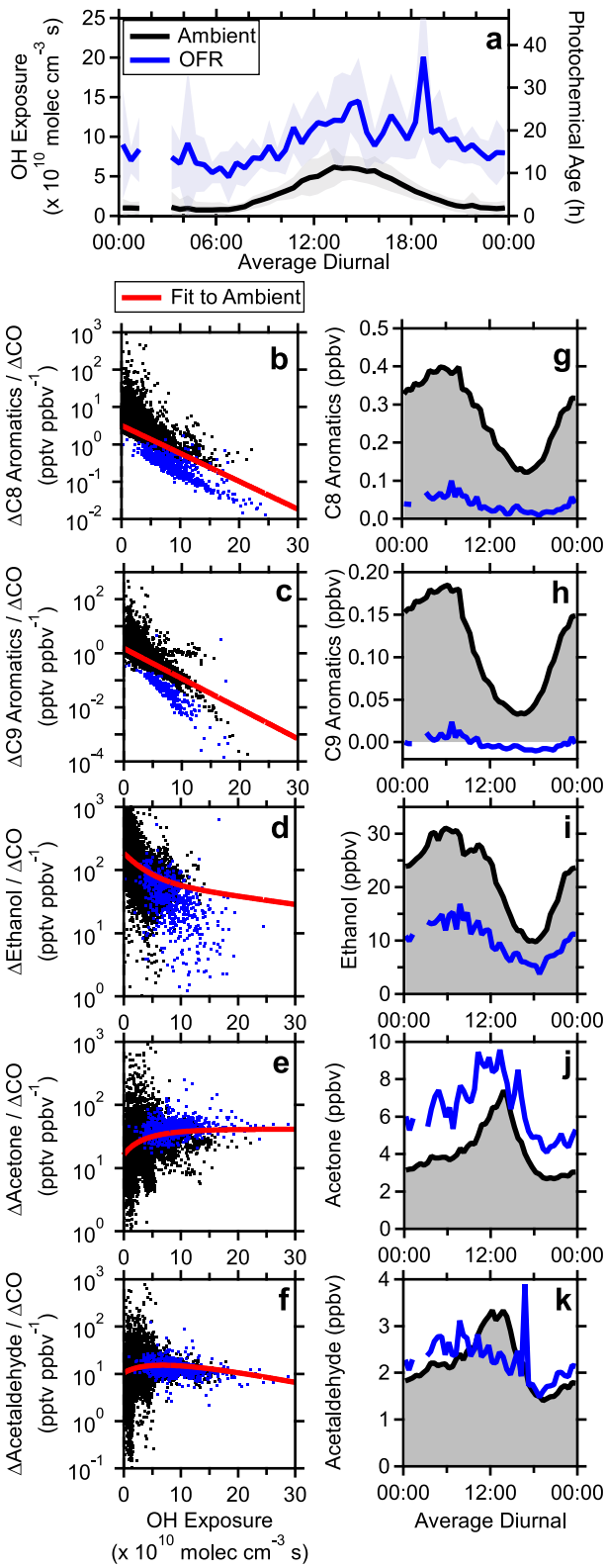


**Figure 9.** Average diurnals of ambient and OFR OH exposure with estimated photochemical age ([OH] = $1.5 \times 10^6$ molec $cm^{-3}$) (a), and multivariate fits of selected VOCs in both ambient air and downstream of the OFR (b–f) and the corresponding diurnal averages (g–k).

exposures. This is important as the aging of air masses does not stop in Pasadena, and these measurements provide insight into the chemical transformations further downwind. Moreover, future evolutions in precursor emissions, temperature, and photochemistry may lead to higher OH exposure levels in the LA basin.

Generally, the oxidation of precursors and the formation of products behave as expected in the OFR. The OFR-Vocus measurements agree well with the multivariate fits of the ambient data within limitations of the measurements. Additionally, there is some overlap in OH exposure between the least oxidized OFR measurements at night, and the highest OH exposure ambient measurements during the day. The oxidation of nighttime ambient air by the OFR serves as a surrogate for daytime ambient oxidation, as described by Ortega et al. (2016). There appears to be an offset between the OFR- and RT-Vocus enhancements, particularly for C8 and C9 aromatics. Experiments with a dark OFR and no additional chemistry suggest no significant additional losses to the system. That is, measured concentrations of C8 and C9 aromatics downstream of the dark OFR were within 2 ± 3% and 3 ± 11% of ambient measurements (averaged 1 min before and 1 min after the dark OFR measurements), respectively. Instead, the observed offset may reflect underestimated OH exposure in the OFR arising from the measurement limitations of the Vocus.

Acknowledging this offset, the precursor and product enhancements agree across OFR-Vocus and RT-Vocus measurement within this overlap (Figures 9b–9f). These observations suggest that the OFR accurately represents trends from ambient oxidation of these VOCs, and the multivariate fits are sufficient for describing their emissions and chemistry. Moreover, the gas-phase OFR-Vocus measurements are representative of real atmospheric conditions (at least by these metrics), supporting the use of OFRs to study secondary organic aerosol formation from gas-phase precursors.

Precursors were removed in the OFR to a much greater extent due to the higher OH exposure, leading to the production of more oxidation products. The average diurnals of C8 and C9 aromatics show nearly complete removal by the OFR during the day with mixing ratios reaching the limits of detection at high OH exposure (Figures 9g and 9h). The average diurnals for acetone and acetaldehyde suggest that significant fractions of their precursors are already oxidized (Figures 9j and 9k). Midday, an additional ∼2 ppbv of acetone was produced in the OFR on top of ∼3 ppbv of acetone which was produced through ambient oxidation (Figure 6j). Acetone also reacts with OH, although at a relatively slow rate. Acetaldehyde, however, reacts much faster with OH, such that it is removed by the OFR relative to ambient. Ethanol, being a primary emission, is only reduced by additional OH exposure in the OFR (Figure 9i). Acetaldehyde is produced from the oxidation of ethanol, but the lack of elevated acetaldehyde observations further shows that photochemical losses are outpacing production for acetaldehyde.

The above chemistry is reflected in the multivariate fits. For C8 and C9 aromatics, the fits show a decrease in concentrations as OH exposure increases and precursors react, but the OFR-Vocus measurements of these aromatics reach the limit of detection, causing a divergence between the predicted and measured enhancements at these high OH exposures (Figures 9b and 9c) and complicating the retrieval of OH exposure. As stated previously, OH exposure for the ambient and OFR data were derived using C8 and C9 aromatics and weighted average rate coefficient with OH radicals. As these mixtures

age, they will become less reactive and the OH exposure would likely be underestimated, including for the ambient OH exposure estimations. This issue is possibly exacerbated by the added exposure in the OFR. Ratios of less reactive hydrocarbons may provide a better estimate of OH exposure in the OFR. Nonetheless, these observations show that fresh emissions of these aromatics can be nearly completely oxidized in ~2 days of ambient exposure. At the same time, both acetone and acetaldehyde production reached a maximum at high OH exposure (Figures 9e and 9f). The corresponding precursors for these OVOCs have essentially been entirely oxidized and acetaldehyde began to be oxidized faster than it was formed. Ambient concentrations of both OVOCs are not expected to increase significantly with increasing OH exposure.

## 4. Conclusions

In this study, VOCs were measured in Pasadena, California, in summer 2022 by Vocus-PTR-TOF-MS to assess their emissions and chemistry. Developments in instrumentation have allowed for a greater breadth of VOC measurements at lower concentrations, allowing for a more detailed investigation into primary emissions and secondary formation. We also deployed an OFR, which doubled the ambient OH exposure, to investigate the potential oxidation of precursors and potential formation of OVOCs. The OFR measurement agreed with expectations set by the ambient measurements.

Relative to the earlier CalNex study at the same location in 2010, ambient concentrations of primary criteria pollutants (CO and $NO_x$) and primary anthropogenic VOCs (aromatics) were lower on average and when comparing for similar temperatures. Emission ratios of these precursor VOCs relative to CO have also declined ~20%, suggesting overall reduced emissions from mobile sources. The subset of investigated compounds was also expanded to include some PAHs from traffic and asphalt, and VCPs. PAH emissions and oxidation products have significant implications for secondary organic aerosol formation while VCPs represent a relatively unregulated emission source which is growing in importance. Most precursors tended to have higher nighttime concentrations with the notable exceptions of isoprene and some VCPs with strong evaporative sources.

Ambient concentrations of ozone were comparable between 2022 and 2010 with a ~20% higher peak daytime concentration in 2022. When comparing daytime ozone concentrations at similar temperatures, however, concentrations were lower in 2022 than in 2010. Although concentrations of $NO_x$ and some anthropogenic VOCs have declined in the past decade, the change in total VOCs is unclear and requires further investigation. Additional factors such as meteorology also influence ozone production. These considerations should be carefully examined before a conclusion regarding LA's chemical regime can be made. Regardless, higher average temperatures resulted in generally equivalent average ozone concentrations between 2010 and 2022, and a higher daytime peak ozone concentration in 2022. The higher average temperatures resulted in faster photochemistry and higher average OH exposure. OH exposure was also higher in 2022 than 2010 at similar daytime temperatures. Further reductions in precursor emissions from mobile sources and VCPs may result in reduced ozone formation under similar conditions, but the future climate must also be considered.

OVOC contributions from primary emissions and secondary formation were separately determined. Emission ratios relative to CO were enhanced relative to 2010, possibly due to reduced combustion emissions of CO, increasing amounts of unregulated VCP emissions, and enhanced evaporation from higher average temperatures. The relative importance of the primary emission component has grown for these reasons. OVOCs with more significant primary contributions tended to have higher nighttime concentrations or comparable daytime and nighttime concentrations. Species with more oxygen atoms tended to have much higher daytime concentrations due to strong secondary formation. OFR-Vocus measurements suggest that daytime acetone production is already near maximum (with increasing OH exposure) and further OH exposure can reduce acetaldehyde below ambient concentrations. Faster photochemistry may not only produce OVOCs more quickly but also remove them more quickly.

The average daytime uncalibrated signal of all species measured by the Vocus was ~11% higher than the average nighttime signal, suggesting that primarily daytime emission sources, such as evaporation, and daytime chemistry contribute more to the measured VOC burden than other, primarily nighttime emission sources and nighttime chemistry. These measurements were made in the summer when evaporative emissions and daytime chemistry are greatest, so this burden is expected to shift toward other sources during cooler months.

## Conflict of Interest

The authors declare no conflicts of interest relevant to this study.

## Data Availability Statement

The CalNexT-2022 data presented in this manuscript are publicly available on the Open Science Framework: https://doi.org/10.17605/OSF.IO/FBSKP (Jensen et al., 2024). CalNex-2010 data were obtained from the National Oceanic and Atmospheric Administration Chemical Sciences Laboratory data repository (US Department of Commerce, 2011).

**Acknowledgments**
Funding for the University of Colorado Boulder contributions was provided by a grant from the National Science Foundation (#2206655). MM was partially supported by a CIRES Innovative Research Program project. Funding for the Caltech and University of California Irvine contributions was provided by NOAA via NA21OAR4310224 and NA21OAR4310222, respectively. The authors would like to thank the supporting members from the University of Colorado, Caltech, and the University of California Irvine for their help with establishing and maintaining the measurement site.

## References

Alton, M. W., & Browne, E. C. (2020). Atmospheric chemistry of volatile methyl siloxanes: Kinetics and products of oxidation by OH radicals and Cl atoms. *Environmental Science & Technology*, *54*(10), 5992–5999. https://doi.org/10.1021/acs.est.0c01368

Aschmann, S. M., Arey, J., & Atkinson, R. (2013). Rate constants for the reactions of OH radicals with 1,2,4,5-Tetramethylbenzene, Pentamethylbenzene, 2,4,5-Trimethylbenzaldehyde, 2,4,5-Trimethylphenol, and 3-Methyl-3-hexene-2,5-dione and products of OH + 1,2,4,5-Tetramethylbenzene. *The Journal of Physical Chemistry A*, *117*(12), 2556–2568. https://doi.org/10.1021/jp400323n

Atkinson, R. (1986). Kinetics and mechanisms of the gas-phase reactions of the hydroxyl radical with organic compounds under atmospheric conditions. *Chemical Reviews*, *86*(1), 69–201. https://doi.org/10.1021/cr00071a004

Atkinson, R., & Arey, J. (2003). Atmospheric degradation of volatile organic compounds. *Chemical Reviews*, *103*(12), 4605–4638. https://doi.org/10.1021/cr0206420

Atkinson, R., Aschmann, S. M., Winer, A. M., & Pitts, J. N. (1985). Atmospheric gas phase loss processes for chlorobenzene, benzotrifluoride, and 4-chlorobenzotrifluoride, and generalization of predictive techniques for atmospheric lifetimes of aromatic compounds. *Archives of Environmental Contamination and Toxicology*, *14*(4), 417–425. https://doi.org/10.1007/BF01055527

Atkinson, R., Baulch, D. L., Cox, R. A., Hampson, R. F., Kerr, J. A., Rossi, M. J., & Troe, J. (1997). Evaluated kinetic, photochemical and heterogeneous data for atmospheric chemistry: Supplement V. IUPAC subcommittee on gas kinetic data evaluation for atmospheric chemistry. *Journal of Physical and Chemical Reference Data*, *26*(3), 521–1011. https://doi.org/10.1063/1.556011

Borbon, A., Dominutti, P., Panopoulou, A., Gros, V., Sauvage, S., Farhat, M., et al. (2023). Ubiquity of anthropogenic terpenoids in cities worldwide: Emission ratios, emission quantification and implications for urban atmospheric chemistry. *Journal of Geophysical Research: Atmospheres*, *128*(7), e2022JD037566. https://doi.org/10.1029/2022JD037566

Borbon, A., Gilman, J. B., Kuster, W. C., Grand, N., Chevaillier, S., Colomb, A., et al. (2013). Emission ratios of anthropogenic volatile organic compounds in northern mid-latitude megacities: Observations versus emission inventories in Los Angeles and Paris. *Journal of Geophysical Research: Atmospheres*, *118*(4), 2041–2057. https://doi.org/10.1002/jgrd.50059

Brune, W. H. (2019). The chamber wall index for gas–Wall interactions in atmospheric environmental enclosures. *Environmental Science & Technology*, *53*(7), 3645–3652. https://doi.org/10.1021/acs.est.8b06260

Buchholz, R. R., Worden, H. M., Park, M., Francis, G., Deeter, M. N., Edwards, D. P., et al. (2021). Air pollution trends measured from Terra: CO and AOD over industrial, fire-prone, and background regions. *Remote Sensing of Environment*, *256*, 112275. https://doi.org/10.1016/j.rse.2020.112275

Buhr, K., van Ruth, S., & Delahunty, C. (2002). Analysis of volatile flavour compounds by proton transfer reaction-mass spectrometry: Fragmentation patterns and discrimination between isobaric and isomeric compounds. *International Journal of Mass Spectrometry*, *221*(1), 1–7. https://doi.org/10.1016/S1387-3806(02)00896-5

Cao, C., Gentner, D. R., Commane, R., Toledo-Crow, R., Schiferl, L. D., & Mak, J. E. (2023). Policy-related gains in urban air quality may be offset by increased emissions in a warming climate. *Environmental Science & Technology*, *57*(26), 9683–9692. https://doi.org/10.1021/acs.est.2c05904

Cappellin, L., Karl, T., Probst, M., Ismailova, O., Winkler, P. M., Soukoulis, C., et al. (2012). On quantitative determination of volatile organic compound concentrations using proton transfer reaction time-of-flight mass spectrometry. *Environmental Science & Technology*, *46*(4), 2283–2290. https://doi.org/10.1021/es203985t

Cappellin, L., Probst, M., Limtrakul, J., Biasioli, F., Schuhfried, E., Soukoulis, C., et al. (2010). Proton transfer reaction rate coefficients between $H_3O^+$ and some sulphur compounds. *International Journal of Mass Spectrometry*, *295*(1), 43–48. https://doi.org/10.1016/j.ijms.2010.06.023

Carpenter, L. J., Archer, S. D., & Beale, R. (2012). Ocean-atmosphere trace gas exchange. *Chemical Society Reviews*, *41*(19), 6473–6506. https://doi.org/10.1039/C2CS35121H

Chameides, W. L., Fehsenfeld, F., Rodgers, M. O., Cardelino, C., Martinez, J., Parrish, D., et al. (1992). Ozone precursor relationships in the ambient atmosphere. *Journal of Geophysical Research*, *97*(D5), 6037–6055. https://doi.org/10.1029/91JD03014

Chattopadhyay, A., Bedjanian, Y., Romanias, M. N., Eleftheriou, A. D., Melissas, V. S., Papadimitriou, V. C., & Burkholder, J. B. (2022). OH radical and chlorine atom kinetics of substituted aromatic compounds: 4-Chlorobenzotrifluoride (p-ClC6H4CF3). *The Journal of Physical Chemistry A*, *126*(32), 5407–5419. https://doi.org/10.1021/acs.jpca.2c04455

Chen, T.-M., Kuschner, W. G., Gokhale, J., & Shofer, S. (2007). Outdoor air pollution: Ozone health effects. *The American Journal of the Medical Sciences*, *333*(4), 244–248. https://doi.org/10.1097/MAJ.0b013e31803b8e8c

Chesnavich, W. J., Su, T., & Bowers, M. T. (1980). Collisions in a noncentral field: A variational and trajectory investigation of ion–dipole capture. *The Journal of Chemical Physics*, *72*(4), 2641–2655. https://doi.org/10.1063/1.439409

Claflin, M. S., Pagonis, D., Finewax, Z., Handschy, A. V., Day, D. A., Brown, W. L., et al. (2021). An in situ gas chromatograph with automatic detector switching between PTR- and EI-TOF-MS: Isomer-resolved measurements of indoor air. *Atmospheric Measurement Techniques*, *14*(1), 133–152. https://doi.org/10.5194/amt-14-133-2021

Clairotte, M., Adam, T. W., Zardini, A. A., Manfredi, U., Martini, G., Krasenbrink, A., et al. (2013). Effects of low temperature on the cold start gaseous emissions from light duty vehicles fuelled by ethanol-blended gasoline. *Applied Energy*, *102*, 44–54. https://doi.org/10.1016/j.apenergy.2012.08.010

Coggon, M. M., Gkatzelis, G. I., McDonald, B. C., Gilman, J. B., Schwantes, R. H., Abuhassan, N., et al. (2021). Volatile chemical product emissions enhance ozone and modulate urban chemistry. *Proceedings of the National Academy of Sciences*, *118*(32), e2026653118. https://doi.org/10.1073/pnas.2026653118

Coggon, M. M., Stockwell, C. E., Claflin, M. S., Pfannerstill, E. Y., Xu, L., Gilman, J. B., et al. (2024). Identifying and correcting interferences to PTR-ToF-MS measurements of isoprene and other urban volatile organic compounds. *Atmospheric Measurement Techniques*, *17*(2), 801–825. https://doi.org/10.5194/amt-17-801-2024

Coggon, M. M., Stockwell, C. E., Xu, L., Peischl, J., Gilman, J. B., Lamplugh, A., et al. (2024). Contribution of cooking emissions to the urban volatile organic compounds in Las Vegas, NV. *Atmospheric Chemistry and Physics*, *24*(7), 4289–4304. https://doi.org/10.5194/acp-24-4289-2024

Coggon, M. M., Veres, P. R., Yuan, B., Koss, A., Warneke, C., Gilman, J. B., et al. (2016). Emissions of nitrogen-containing organic compounds from the burning of herbaceous and arboraceous biomass: Fuel composition dependence and the variability of commonly used nitrile tracers. *Geophysical Research Letters*, *43*(18), 9903–9912. https://doi.org/10.1002/2016GL070562

Colman, J. J., Swanson, A. L., Meinardi, S., Sive, B. C., Blake, D. R., & Rowland, F. S. (2001). Description of the analysis of a wide range of volatile organic compounds in whole air samples collected during PEM-tropics A and B. *Analytical Chemistry*, *73*(15), 3723–3731. https://doi.org/10.1021/ac010027g

Cubison, M. J., & Jimenez, J. L. (2015). Statistical precision of the intensities retrieved from constrained fitting of overlapping peaks in high-resolution mass spectra. *Atmospheric Measurement Techniques*, *8*(6), 2333–2345. https://doi.org/10.5194/amt-8-2333-2015

Day, D. A., Fry, J. L., Kang, H. G., Krechmer, J. E., Ayres, B. R., Keehan, N. I., et al. (2022). Secondary organic aerosol mass yields from $NO_3$ oxidation of α-Pinene and Δ-Carene: Effect of $RO_2$ radical fate. *The Journal of Physical Chemistry A*, *126*(40), 7309–7330. https://doi.org/10.1021/acs.jpca.2c04419

de Gouw, J. A., Gilman, J. B., Kim, S.-W., Alvarez, S. L., Dusanter, S., Graus, M., et al. (2018). Chemistry of volatile organic compounds in the Los Angeles Basin: Formation of oxygenated compounds and determination of emission ratios. *Journal of Geophysical Research: Atmospheres*, *123*(4), 2298–2319. https://doi.org/10.1002/2017JD027976

de Gouw, J. A., Gilman, J. B., Kim, S.-W., Lerner, B. M., Isaacman-VanWertz, G., McDonald, B. C., et al. (2017). Chemistry of volatile organic compounds in the Los Angeles basin: Nighttime removal of alkenes and determination of emission ratios. *Journal of Geophysical Research: Atmospheres*, *122*(21), 11843–11861. https://doi.org/10.1002/2017JD027459

de Gouw, J. A., Middlebrook, A. M., Warneke, C., Ahmadov, R., Atlas, E. L., Bahreini, R., et al. (2011). Organic aerosol formation downwind from the Deepwater Horizon oil spill. *Science*, *331*(6022), 1295–1299. https://doi.org/10.1126/science.1200320

de Gouw, J. A., Middlebrook, A. M., Warneke, C., Goldan, P. D., Kuster, W. C., Roberts, J. M., et al. (2005). Budget of organic carbon in a polluted atmosphere: Results from the New England air quality study in 2002. *Journal of Geophysical Research*, *110*(D16), D16305. https://doi.org/10.1029/2004JD005623

Derwent, R. G., Jenkin, M. E., & Saunders, S. M. (1996). Photochemical ozone creation potentials for a large number of reactive hydrocarbons under European conditions. *Atmospheric Environment*, *30*(2), 181–199. https://doi.org/10.1016/1352-2310(95)00303-G

DeVault, M. P., Ziola, A. C., & Ziemann, P. J. (2022). Products and mechanisms of secondary organic aerosol formation from the $NO_3$ radical-initiated oxidation of cyclic and acyclic monoterpenes. *ACS Earth and Space Chemistry*, *6*(8), 2076–2092. https://doi.org/10.1021/acsearthspacechem.2c00130

Drozd, G. T., Zhao, Y., Saliba, G., Frodin, B., Maddox, C., Weber, R. J., et al. (2016). Time resolved measurements of speciated tailpipe emissions from motor vehicles: Trends with emission control technology, cold start effects, and speciation. *Environmental Science & Technology*, *50*(24), 13592–13599. https://doi.org/10.1021/acs.est.6b04513

Dzepina, K., Volkamer, R. M., Madronich, S., Tulet, P., Ulbrich, I. M., Zhang, Q., et al. (2009). Evaluation of recently-proposed secondary organic aerosol models for a case study in Mexico City. *Atmospheric Chemistry and Physics*, *9*(15), 5681–5709. https://doi.org/10.5194/acp-9-5681-2009

Ensberg, J. J., Hayes, P. L., Jimenez, J. L., Gilman, J. B., Kuster, W. C., de Gouw, J. A., et al. (2014). Emission factor ratios, SOA mass yields, and the impact of vehicular emissions on SOA formation. *Atmospheric Chemistry and Physics*, *14*(5), 2383–2397. https://doi.org/10.5194/acp-14-2383-2014

Fu, Y., Li, W., Manheim, J. M., Milton, J., Kilaz, G., & Kenttämaa, H. I. (2022). Proton affinities of alkanes. *Journal of the American Society for Mass Spectrometry*, *33*(10), 1850–1857. https://doi.org/10.1021/jasms.2c00152

Fujita, E. M., Campbell, D. E., Stockwell, W. R., & Lawson, D. R. (2013). Past and future ozone trends in California's South Coast Air Basin: Reconciliation of ambient measurements with past and projected emission inventories. *Journal of the Air & Waste Management Association*, *63*(1), 54–69. https://doi.org/10.1080/10962247.2012.735211

Garcia, E., Johnston, J., McConnell, R., Palinkas, L., & Eckel, S. P. (2023). California's early transition to electric vehicles: Observed health and air quality co-benefits. *Science of the Total Environment*, *867*, 161761. https://doi.org/10.1016/j.scitotenv.2023.161761

Gilman, J. B., Lerner, B. M., Kuster, W. C., Goldan, P. D., Warneke, C., Veres, P. R., et al. (2015). Biomass burning emissions and potential air quality impacts of volatile organic compounds and other trace gases from fuels common in the US. *Atmospheric Chemistry and Physics*, *15*(24), 13915–13938. https://doi.org/10.5194/acp-15-13915-2015

Gkatzelis, G. I., Coggon, M. M., McDonald, B. C., Peischl, J., Aikin, K. C., Gilman, J. B., et al. (2021). Identifying volatile chemical product tracer compounds in U.S. cities. *Environmental Science & Technology*, *55*(1), 188–199. https://doi.org/10.1021/acs.est.0c05467

Gkatzelis, G. I., Coggon, M. M., McDonald, B. C., Peischl, J., Gilman, J. B., Aikin, K. C., et al. (2021). Observations confirm that volatile chemical products are a major source of petrochemical emissions in U.S. cities. *Environmental Science & Technology*, *55*(8), 4332–4343. https://doi.org/10.1021/acs.est.0c05471

Goldberg, D. L., Anenberg, S. C., Griffin, D., McLinden, C. A., Lu, Z., & Streets, D. G. (2020). Disentangling the impact of the COVID-19 lockdowns on urban $NO_2$ from natural variability. *Geophysical Research Letters*, *47*(17), e2020GL089269. https://doi.org/10.1029/2020GL089269

Graus, M., Müller, M., & Hansel, A. (2010). High resolution PTR-TOF: Quantification and formula confirmation of VOC in real time. *Journal of the American Society for Mass Spectrometry*, *21*(6), 1037–1044. https://doi.org/10.1016/j.jasms.2010.02.006

Griffith, S. M., Hansen, R. F., Dusanter, S., Michoud, V., Gilman, J. B., Kuster, W. C., et al. (2016). Measurements of hydroxyl and hydroperoxy radicals during CalNex-LA: Model comparisons and radical budgets. *Journal of Geophysical Research: Atmospheres*, *121*(8), 4211–4232. https://doi.org/10.1002/2015JD024358

Gu, S., Guenther, A., & Faiola, C. (2021). Effects of anthropogenic and biogenic volatile organic compounds on Los Angeles air quality. *Environmental Science & Technology*, *55*(18), 12191–12201. https://doi.org/10.1021/acs.est.1c01481

Gu, S., Luo, W., Charmchi, A., McWhirter, K. J., Rosenstiel, T., Pankow, J., & Faiola, C. L. (2024). Limonene enantiomeric ratios from anthropogenic and biogenic emission sources. *Environmental Science and Technology Letters*, *11*(2), 130–135. https://doi.org/10.1021/acs.estlett.3c00794

Gueneron, M., Erickson, M. H., VanderSchelden, G. S., & Jobson, B. T. (2015). PTR-MS fragmentation patterns of gasoline hydrocarbons. *International Journal of Mass Spectrometry*, *379*, 97–109. https://doi.org/10.1016/j.ijms.2015.01.001

Hantschke, L., Novelli, A., Bohn, B., Cho, C., Reimer, D., Rohrer, F., et al. (2021). Atmospheric photooxidation and ozonolysis of $\Delta^3$-carene and 3-caronaldehyde: Rate constants and product yields. *Atmospheric Chemistry and Physics*, *21*(16), 12665–12685. https://doi.org/10.5194/acp-21-12665-2021

Hayes, P. L., Ortega, A. M., Cubison, M. J., Froyd, K. D., Zhao, Y., Cliff, S. S., et al. (2013). Organic aerosol composition and sources in Pasadena, California, during the 2010 CalNex campaign. *Journal of Geophysical Research: Atmospheres*, *118*(16), 9233–9257. https://doi.org/10.1002/jgrd.50530

Haynes, W. M. (Ed.) (2014)., *CRC handbook of chemistry and physics* (95th ed.). CRC Press.

Helmig, D. (1997). Ozone removal techniques in the sampling of atmospheric volatile organic trace gases. *Atmospheric Environment*, *31*(21), 3635–3651. https://doi.org/10.1016/S1352-2310(97)00144-1

Isaacman-VanWertz, G., Lerner, B. M., & Sueper, D. T. (2022). *TERN v2.2.20*. Zenodo. https://doi.org/10.5281/zenodo.6940761

Isaacman-VanWertz, G., Sueper, D. T., Aikin, K. C., Lerner, B. M., Gilman, J. B., de Gouw, J. A., et al. (2017). Automated single-ion peak fitting as an efficient approach for analyzing complex chromatographic data. *Journal of Chromatography A*, *1529*, 81–92. https://doi.org/10.1016/j.chroma.2017.11.005

Jacob, D. J. (1999). *Introduction to atmospheric chemistry* (Illustrated edition). Princeton University Press.

Jenkin, M. E., Saunders, S. M., & Pilling, M. J. (1997). The tropospheric degradation of volatile organic compounds: A protocol for mechanism development. *Atmospheric Environment*, *31*(1), 81–104. https://doi.org/10.1016/S1352-2310(96)00105-7

Jenks, O. J., DeVault, M. P., Ziola, A. C., Morris, M. A., Schueneman, M. K., Stark, H., et al. (2023). Investigation of gas-phase products from the $NO_3$ radical oxidation of Δ-3-Carene. *ACS Earth and Space Chemistry*, *7*(5), 1097–1106. https://doi.org/10.1021/acsearthspacechem.3c00020

Jensen, A. R., Koss, A. R., Hales, R. B., & de Gouw, J. A. (2023). Measurements of volatile organic compounds in ambient air by gas-chromatography and real-time Vocus PTR-TOF-MS: Calibrations, instrument background corrections, and introducing a PTR data toolkit. *Atmospheric Measurement Techniques*, *16*(21), 5261–5285. https://doi.org/10.5194/amt-16-5261-2023

Jensen, A. R., Morris, M. A., Schulze, B. C., Bradley, A. C., Anderson, L. D., Jenks, O. J., et al. (2024). Volatile organic compound measurements in Pasadena, CA Jul-Aug 2022 [Dataset]. *OSF*. https://doi.org/10.17605/OSF.IO/FBSKP

Jordan, A., Haidacher, S., Hanel, G., Hartungen, E., Märk, L., Seehauser, H., et al. (2009). A high resolution and high sensitivity proton-transfer-reaction time-of-flight mass spectrometer (PTR-TOF-MS). *International Journal of Mass Spectrometry*, *286*(2), 122–128. https://doi.org/10.1016/j.ijms.2009.07.005

Kang, E., Root, M. J., Toohey, D. W., & Brune, W. H. (2007). Introducing the concept of potential aerosol mass (PAM). *Atmospheric Chemistry and Physics*, *7*(22), 5727–5744. https://doi.org/10.5194/acp-7-5727-2007

Khare, P., Machesky, J., Soto, R., He, M., Presto, A. A., & Gentner, D. R. (2020). Asphalt-related emissions are a major missing nontraditional source of secondary organic aerosol precursors. *Science Advances*, *6*(36), eabb9785. https://doi.org/10.1126/sciadv.abb9785

Kilgour, D. B., Novak, G. A., Claflin, M. S., Lerner, B. M., & Bertram, T. H. (2024). Production of oxygenated volatile organic compounds from the ozonolysis of coastal seawater. *Atmospheric Chemistry and Physics*, *24*(6), 3729–3742. https://doi.org/10.5194/acp-24-3729-2024

Kim, S.-W., McDonald, B. C., Seo, S., Kim, K.-M., & Trainer, M. (2022). Understanding the paths of surface ozone abatement in the Los Angeles Basin. *Journal of Geophysical Research: Atmospheres*, *127*(4), e2021JD035606. https://doi.org/10.1029/2021JD035606

Klein, F., Platt, S. M., Farren, N. J., Detournay, A., Bruns, E. A., Bozzetti, C., et al. (2016). Characterization of gas-phase organics using proton transfer reaction time-of-flight mass spectrometry: Cooking emissions. *Environmental Science & Technology*, *50*(3), 1243–1250. https://doi.org/10.1021/acs.est.5b04618

Koss, A. R., Sekimoto, K., Gilman, J. B., Selimovic, V., Coggon, M. M., Zarzana, K. J., et al. (2018). Non-methane organic gas emissions from biomass burning: Identification, quantification, and emission factors from PTR-ToF during the FIREX 2016 laboratory experiment. *Atmospheric Chemistry and Physics*, *18*(5), 3299–3319. https://doi.org/10.5194/acp-18-3299-2018

Krechmer, J., Lopez-Hilfiker, F., Koss, A., Hutterli, M., Stoermer, C., Deming, B., et al. (2018). Evaluation of a new reagent-ion source and focusing ion–molecule reactor for use in proton-transfer-reaction mass spectrometry. *Analytical Chemistry*, *90*(20), 12011–12018. https://doi.org/10.1021/acs.analchem.8b02641

Kurpius, M. R., & Goldstein, A. H. (2003). Gas-phase chemistry dominates $O_3$ loss to a forest, implying a source of aerosols and hydroxyl radicals to the atmosphere. *Geophysical Research Letters*, *30*(7), 1371. https://doi.org/10.1029/2002GL016785

Kwok, E. S. C., Atkinson, R., & Arey, J. (1997). Kinetics of the gas-phase reactions of indan, indene, fluorene, and 9,10-dihydroanthracene with OH radicals, $NO_3$ radicals, and $O_3$. *International Journal of Chemical Kinetics*, *29*(4), 299–309. https://doi.org/10.1002/(SICI)1097-4601(1997)29:4<299::AID-KIN9>3.0.CO;2-P

Lambe, A. T., Ahern, A. T., Williams, L. R., Slowik, J. G., Wong, J. P. S., Abbatt, J. P. D., et al. (2011). Characterization of aerosol photooxidation flow reactors: Heterogeneous oxidation, secondary organic aerosol formation and cloud condensation nuclei activity measurements. *Atmospheric Measurement Techniques*, *4*(3), 445–461. https://doi.org/10.5194/amt-4-445-2011

Langevin, P. (1905). A fundamental formula of kinetic theory. *Annales de Chimie et de Physique*, *5*, 245–288.

Langford, V. S., Gray, J. D. C., & McEwan, M. J. (2013). Selected ion flow tube studies of several siloxanes. *Rapid Communications in Mass Spectrometry*, *27*(6), 700–706. https://doi.org/10.1002/rcm.6496

Lerner, B. M., Gilman, J. B., Aikin, K. C., Atlas, E. L., Goldan, P. D., Graus, M., et al. (2017). An improved, automated whole air sampler and gas chromatography mass spectrometry analysis system for volatile organic compounds in the atmosphere. *Atmospheric Measurement Techniques*, *10*(1), 291–313. https://doi.org/10.5194/amt-10-291-2017

Li, R., Palm, B. B., Borbon, A., Graus, M., Warneke, C., Ortega, A. M., et al. (2013). Laboratory studies on secondary organic aerosol formation from crude oil vapors. *Environmental Science & Technology*, *47*(21), 12566–12574. https://doi.org/10.1021/es402265y

Li, R., Palm, B. B., Ortega, A. M., Hlywiak, J., Hu, W., Peng, Z., et al. (2015). Modeling the radical chemistry in an oxidation flow reactor: Radical formation and recycling, sensitivities, and the oh exposure estimation equation. *The Journal of Physical Chemistry A*, *119*(19), 4418–4432. https://doi.org/10.1021/jp509534k

Li, Z., Ratliff, E. A., & Sharkey, T. D. (2011). Effect of temperature on postillumination isoprene emission in oak and poplar1[OA]. *Plant Physiology*, *155*(2), 1037–1046. https://doi.org/10.1104/pp.110.167551

Liggio, J., Li, S.-M., Hayden, K., Taha, Y. M., Stroud, C., Darlington, A., et al. (2016). Oil sands operations as a large source of secondary organic aerosols. *Nature*, *534*(7605), 91–94. https://doi.org/10.1038/nature17646

Liu, G., Ma, X., Li, W., Chen, J., Ji, Y., & An, T. (2024). Pollution characteristics, source appointment and environmental effect of oxygenated volatile organic compounds in Guangdong-Hong Kong-Macao Greater Bay Area: Implication for air quality management. *Science of the Total Environment*, *919*, 170836. https://doi.org/10.1016/j.scitotenv.2024.170836

Liu, P., Wu, Y., Li, Z., Lv, Z., Zhang, J., Liu, Y., et al. (2024). Tailpipe volatile organic compounds (VOCs) emissions from Chinese gasoline vehicles under different vehicle standards, fuel types, and driving conditions. *Atmospheric Environment*, *323*, 120348. https://doi.org/10.1016/j.atmosenv.2024.120348

Mao, J., Ren, X., Brune, W. H., Olson, J. R., Crawford, J. H., Fried, A., et al. (2009). Airborne measurement of OH reactivity during INTEX-B. *Atmospheric Chemistry and Physics*, *9*(1), 163–173. https://doi.org/10.5194/acp-9-163-2009

McDonald, B. C., Dallmann, T. R., Martin, E. W., & Harley, R. A. (2012). Long-term trends in nitrogen oxide emissions from motor vehicles at national, state, and air basin scales. *Journal of Geophysical Research*, *117*(D21), D00V18. https://doi.org/10.1029/2012JD018304

McDonald, B. C., de Gouw, J. A., Gilman, J. B., Jathar, S. H., Akherati, A., Cappa, C. D., et al. (2018). Volatile chemical products emerging as largest petrochemical source of urban organic emissions. *Science*, *359*(6377), 760–764. https://doi.org/10.1126/science.aaq0524

National Research Council. (2004). *Air quality management in the United States*. National Academies Press. https://doi.org/10.17226/10728

Nussbaumer, C. M., & Cohen, R. C. (2020). The role of temperature and NOx in ozone trends in the Los Angeles Basin. *Environmental Science & Technology*, *54*(24), 15652–15659. https://doi.org/10.1021/acs.est.0c04910

Nuvolone, D., Petri, D., & Voller, F. (2018). The effects of ozone on human health. *Environmental Science and Pollution Research*, *25*(9), 8074–8088. https://doi.org/10.1007/s11356-017-9239-3

Ortega, A. M., Hayes, P. L., Peng, Z., Palm, B. B., Hu, W., Day, D. A., et al. (2016). Real-time measurements of secondary organic aerosol formation and aging from ambient air in an oxidation flow reactor in the Los Angeles area. *Atmospheric Chemistry and Physics*, *16*(11), 7411–7433. https://doi.org/10.5194/acp-16-7411-2016

Pagonis, D., Sekimoto, K., & de Gouw, J. A. (2019). A library of proton-transfer reactions of $H_3O^+$ ions used for trace gas detection. *Journal of the American Society for Mass Spectrometry*, *30*(7), 1330–1335. https://doi.org/10.1007/s13361-019-02209-3

Parker, H., Hasheminassab, S., Crounse, J. D., Roehl, C. M., & Wennberg, P. O. (2020). Impacts of traffic reductions associated with COVID-19 on southern California air quality. *Geophysical Research Letters*, *47*(23), e2020GL090164. https://doi.org/10.1029/2020GL090164

Parker, L., Johnson, J., Grant, J., Vennam, P., Parikh, R., Chien, C.-J., & Morris, R. (2022). Ozone trends and the ability of models to reproduce the 2020 ozone concentrations in the south coast air basin in Southern California under the COVID-19 restrictions. *Atmosphere*, *13*(4), 528. https://doi.org/10.3390/atmos13040528

Parrish, D. D., Xu, J., Croes, B., & Shao, M. (2016). Air quality improvement in Los Angeles—Perspectives for developing cities. *Frontiers of Environmental Science & Engineering*, *10*(5), 11. https://doi.org/10.1007/s11783-016-0859-5

Peng, Z., Day, D. A., Ortega, A. M., Palm, B. B., Hu, W., Stark, H., et al. (2016). Non-OH chemistry in oxidation flow reactors for the study of atmospheric chemistry systematically examined by modeling. *Atmospheric Chemistry and Physics*, *16*(7), 4283–4305. https://doi.org/10.5194/acp-16-4283-2016

Peng, Z., & Jimenez, J. L. (2020). Radical chemistry in oxidation flow reactors for atmospheric chemistry research. *Chemical Society Reviews*, *49*(9), 2570–2616. https://doi.org/10.1039/C9CS00766K

Peron, A., Graus, M., Striednig, M., Lamprecht, C., Wohlfahrt, G., & Karl, T. (2024). Deciphering anthropogenic and biogenic contributions to selected non-methane volatile organic compound emissions in an urban area. *Atmospheric Chemistry and Physics*, *24*(12), 7063–7083. https://doi.org/10.5194/acp-24-7063-2024

Pfannerstill, E. Y., Arata, C., Zhu, Q., Schulze, B. C., Ward, R., Woods, R., et al. (2024). Temperature-dependent emissions dominate aerosol and ozone formation in Los Angeles. *Science*, *384*(6702), 1324–1329. https://doi.org/10.1126/science.adg8204

Phousongphouang, P. T., & Arey, J. (2002). Rate constants for the gas-phase reactions of a series of alkylnaphthalenes with the OH radical. *Environmental Science & Technology*, *36*(9), 1947–1952. https://doi.org/10.1021/es011434c

Pollack, I. B., Ryerson, T. B., Trainer, M., Neuman, J. A., Roberts, J. M., & Parrish, D. D. (2013). Trends in ozone, its precursors, and related secondary oxidation products in Los Angeles, California: A synthesis of measurements from 1960 to 2010. *Journal of Geophysical Research: Atmospheres*, *118*(11), 5893–5911. https://doi.org/10.1002/jgrd.50472

Pusede, S. E., Steiner, A. L., & Cohen, R. C. (2015). Temperature and recent trends in the chemistry of continental surface ozone. *Chemical Reviews*, *115*(10), 3898–3918. https://doi.org/10.1021/cr5006815

Rasulov, B., Hüve, K., Bichele, I., Laisk, A., & Niinemets, Ü. (2010). Temperature response of isoprene emission in vivo reflects a combined effect of substrate limitations and isoprene synthase activity: A kinetic analysis. *Plant Physiology*, *154*(3), 1558–1570. https://doi.org/10.1104/pp.110.162081

Reisen, F., & Arey, J. (2002). Reactions of hydroxyl radicals and ozone with acenaphthene and acenaphthylene. *Environmental Science & Technology*, *36*(20), 4302–4311. https://doi.org/10.1021/es025761b

Roberts, J. M., Fehsenfeld, F. C., Liu, S. C., Bollinger, M. J., Hahn, C., Albritton, D. L., & Sievers, R. E. (1984). Measurements of aromatic hydrocarbon ratios and NOx concentrations in the rural troposphere: Observation of air mass photochemical aging and NOx removal. *Atmospheric Environment*, *18*(11), 2421–2432. https://doi.org/10.1016/0004-6981(84)90012-X

Robinson, A. L., Donahue, N. M., Shrivastava, M. K., Weitkamp, E. A., Sage, A. M., Grieshop, A. P., et al. (2007). Rethinking organic aerosols: Semivolatile emissions and photochemical Aging. *Science*, *315*(5816), 1259–1262. https://doi.org/10.1126/science.1133061

Ryerson, T. B., Andrews, A. E., Angevine, W. M., Bates, T. S., Brock, C. A., Cairns, B., et al. (2013). The 2010 California research at the nexus of air quality and climate change (CalNex) field study. *Journal of Geophysical Research: Atmospheres*, *118*(11), 5830–5866. https://doi.org/10.1002/jgrd.50331

Sanadze, G. A. (2004). Biogenic isoprene (a review). *Russian Journal of Plant Physiology*, *51*(6), 729–741. https://doi.org/10.1023/B:RUPP.0000047821.63354.a4

Saunders, S. M., Jenkin, M. E., Derwent, R. G., & Pilling, M. J. (2003). Protocol for the development of the master chemical mechanism, MCM v3 (Part A): Tropospheric degradation of non-aromatic volatile organic compounds. *Atmospheric Chemistry and Physics*, *3*(1), 161–180. https://doi.org/10.5194/acp-3-161-2003

Schauer, J. J., Kleeman, M. J., Cass, G. R., & Simoneit, B. R. T. (1999). Measurement of emissions from air pollution sources. 1. C1 through C29 organic compounds from meat charbroiling. *Environmental Science & Technology*, *33*(10), 1566–1577. https://doi.org/10.1021/es980076j

Schroeder, J. R., Cai, C., Xu, J., Ridley, D., Lu, J., Bui, N., et al. (2022). Changing ozone sensitivity in the south coast air basin during the COVID-19 period. *Atmospheric Chemistry and Physics*, *22*(19), 12985–13000. https://doi.org/10.5194/acp-22-12985-2022

Sekimoto, K., Koss, A. R., Gilman, J. B., Selimovic, V., Coggon, M. M., Zarzana, K. J., et al. (2018). High- and low-temperature pyrolysis profiles describe volatile organic compound emissions from western US wildfire fuels. *Atmospheric Chemistry and Physics*, *18*(13), 9263–9281. https://doi.org/10.5194/acp-18-9263-2018

Sekimoto, K., Li, S.-M., Yuan, B., Koss, A., Coggon, M., Warneke, C., & de Gouw, J. A. (2017). Calculation of the sensitivity of proton-transfer-reaction mass spectrometry (PTR-MS) for organic trace gases using molecular properties. *International Journal of Mass Spectrometry*, *421*, 71–94. https://doi.org/10.1016/j.ijms.2017.04.006

Seltzer, K. M., Murphy, B. N., Pennington, E. A., Allen, C., Talgo, K., & Pye, H. O. T. (2021). Volatile chemical product enhancements to criteria pollutants in the United States. *Environmental Science & Technology*, *56*(11), 6905–6913. https://doi.org/10.1021/acs.est.1c04298

Španěl, P., & Smith, D. (1997). SIFT studies of the reactions of H3O+, NO+ and O2+ with a series of alcohols. *International Journal of Mass Spectrometry and Ion Processes*, *167–168*, 375–388. https://doi.org/10.1016/S0168-1176(97)00085-2

Stockwell, C. E., Coggon, M. M., Gkatzelis, G. I., Ortega, J., McDonald, B. C., Peischl, J., et al. (2021). Volatile organic compound emissions from solvent- and water-borne coatings – Compositional differences and tracer compound identifications. *Atmospheric Chemistry and Physics*, *21*(8), 6005–6022. https://doi.org/10.5194/acp-21-6005-2021

Su, T. (1994). Parametrization of kinetic energy dependences of ion–polar molecule collision rate constants by trajectory calculations. *The Journal of Chemical Physics*, *100*(6), 4703. https://doi.org/10.1063/1.466255

Su, T., & Chesnavich, W. J. (1982). Parametrization of the ion–polar molecule collision rate constant by trajectory calculations. *The Journal of Chemical Physics*, *76*(10), 5183–5185. https://doi.org/10.1063/1.442828

Swain, D., Tsiang, M., Haugen, M., Singh, D., Charland, A., Rajaratnam, B., & Diffenbaugh, N. (2014). The extraordinary California drought of 2013/2014: Character, context, and the role of climate change [in "Explaining Extremes of 2013 from a Climate Perspective"]. *Bulletin of the American Meteorological Society*, *95*(9), S3–S7. https://doi.org/10.1175/1520-0477-95.9.S1.1

TCCON Weather. (2022). The weather at Caltech. Retrieved from http://tccon-weather.caltech.edu/

Thomsen, D., Thomsen, L. D., Iversen, E. M., Björgvinsdóttir, T. N., Vinther, S. F., Skønager, J. T., et al. (2022). Ozonolysis of α-pinene and Δ3-carene mixtures: Formation of dimers with two precursors. *Environmental Science & Technology*, *56*(23), 16643–16651. https://doi.org/10.1021/acs.est.2c04786

Timonen, H., Cubison, M., Aurela, M., Brus, D., Lihavainen, H., Hillamo, R., et al. (2016). Applications and limitations of constrained high-resolution peak fitting on low resolving power mass spectra from the ToF-ACSM. *Atmospheric Measurement Techniques*, *9*(7), 3263–3281. https://doi.org/10.5194/amt-9-3263-2016

US Department of Commerce. (2011). CalNex 2010 LA ground site. Retrieved from https://csl.noaa.gov/groups/csl7/measurements/2010calnex/Ground/DataDownload/index.php?page=/groups/csl7/measurements/2010calnex/Ground/DataDownload/

US EPA. (2023). USEPA: Air data - Ozone exceedances. Retrieved from https://www.epa.gov/outdoor-air-quality-data/air-data-ozone-exceedances

Van Rooy, P., Tasnia, A., Barletta, B., Buenconsejo, R., Crounse, J. D., Kenseth, C., et al. (2021). Observations of volatile organic compounds in the Los Angeles Basin during COVID-19. *ACS Earth and Space Chemistry*, *5*(11), 3045–3055. https://doi.org/10.1021/acsearthspacechem.1c00248

Vermeuel, M. P., Novak, G. A., Kilgour, D. B., Claflin, M. S., Lerner, B. M., Trowbridge, A. M., et al. (2023). Observations of biogenic volatile organic compounds over a mixed temperate forest during the summer to autumn transition. *Atmospheric Chemistry and Physics*, *23*(7), 4123–4148. https://doi.org/10.5194/acp-23-4123-2023

Wahner, A., & Zetzsch, C. (1983). Rate constants for the addition of hydroxyl to aromatics (benzene, p-chloroaniline, and o-m-and p-dichlorobenzene and the unimolecular decay of the adduct. Kinetics into a quasi-equilibrium. Part 1. *The Journal of Physical Chemistry*, *87*(24), 4945–4951. https://doi.org/10.1021/j150642a036

Wallington, T. J., Anderson, J. E., Dolan, R. H., & Winkler, S. L. (2022). Vehicle emissions and urban air quality: 60 years of progress. *Atmosphere*, *13*(5), 650. https://doi.org/10.3390/atmos13050650

Wang, C., Liggio, J., Wentzell, J. J. B., Jorga, S., Folkerson, A., & Abbatt, J. P. D. (2023). Chloramines as an important photochemical source of chlorine atoms in the urban atmosphere. *Proceedings of the National Academy of Sciences*, *120*(30), e2220889120. https://doi.org/10.1073/pnas.2220889120

Wang, S., Yuan, B., He, X., Cui, R., Song, X., Chen, Y., et al. (2024). Emission characteristics of reactive organic gases (ROGs) from industrial volatile chemical products (VCPs) in the Pearl River Delta (PRD), China. *Atmospheric Chemistry and Physics*, *24*(12), 7101–7121. https://doi.org/10.5194/acp-24-7101-2024

Warneke, C., de Gouw, J. A., Edwards, P. M., Holloway, J. S., Gilman, J. B., Kuster, W. C., et al. (2013). Photochemical aging of volatile organic compounds in the Los Angeles basin: Weekday-weekend effect. *Journal of Geophysical Research: Atmospheres*, *118*(10), 5018–5028. https://doi.org/10.1002/jgrd.50423

Warneke, C., de Gouw, J. A., Holloway, J. S., Peischl, J., Ryerson, T. B., Atlas, E., et al. (2012). Multiyear trends in volatile organic compounds in Los Angeles, California: Five decades of decreasing emissions. *Journal of Geophysical Research*, *117*(D21), D00V17. https://doi.org/10.1029/2012JD017899

Warneke, C., Geiger, F., Edwards, P. M., Dube, W., Pétron, G., Kofler, J., et al. (2014). Volatile organic compound emissions from the oil and natural gas industry in the Uintah Basin, Utah: Oil and gas well pad emissions compared to ambient air composition. *Atmospheric Chemistry and Physics*, *14*(20), 10977–10988. https://doi.org/10.5194/acp-14-10977-2014

Warneke, C., McKeen, S. A., de Gouw, J. A., Goldan, P. D., Kuster, W. C., Holloway, J. S., et al. (2007). Determination of urban volatile organic compound emission ratios and comparison with an emissions database. *Journal of Geophysical Research*, *112*(D10), D10S47. https://doi.org/10.1029/2006JD007930

Wernis, R. A., Kreisberg, N. M., Weber, R. J., Drozd, G. T., & Goldstein, A. H. (2022). Source apportionment of VOCs, IVOCs and SVOCs by positive matrix factorization in suburban Livermore, California. *Atmospheric Chemistry and Physics*, *22*(22), 14987–15019. https://doi.org/10.5194/acp-22-14987-2022

Wolfe, G. M., Thornton, J. A., McKay, M., & Goldstein, A. H. (2011). Forest-atmosphere exchange of ozone: Sensitivity to very reactive biogenic VOC emissions and implications for in-canopy photochemistry. *Atmospheric Chemistry and Physics*, *11*(15), 7875–7891. https://doi.org/10.5194/acp-11-7875-2011

Wu, W., Fu, T.-M., Arnold, S. R., Spracklen, D. V., Zhang, A., Tao, W., et al. (2024). Temperature-dependent evaporative anthropogenic VOC emissions significantly exacerbate regional ozone pollution. *Environmental Science & Technology*, *58*(12), 5430–5441. https://doi.org/10.1021/acs.est.3c09122

Yuan, B., Koss, A., Warneke, C., Gilman, J. B., Lerner, B. M., Stark, H., & de Gouw, J. A. (2016). A high-resolution time-of-flight chemical ionization mass spectrometer utilizing hydronium ions ($H_3O^+$ ToF-CIMS) for measurements of volatile organic compounds in the atmosphere. *Atmospheric Measurement Techniques*, *9*(6), 2735–2752. https://doi.org/10.5194/amt-9-2735-2016

Yuan, B., Koss, A. R., Warneke, C., Coggon, M., Sekimoto, K., & de Gouw, J. A. (2017). Proton-transfer-reaction mass spectrometry: Applications in atmospheric sciences. *Chemical Reviews*, *117*(21), 13187–13229. https://doi.org/10.1021/acs.chemrev.7b00325

Zhao, J., & Zhang, R. (2004). Proton transfer reaction rate constants between hydronium ion (H3O+) and volatile organic compounds. *Atmospheric Environment*, *38*(14), 2177–2185. https://doi.org/10.1016/j.atmosenv.2004.01.019

Zheng, B., Chevallier, F., Yin, Y., Ciais, P., Fortems-Cheiney, A., Deeter, M. N., et al. (2019). Global atmospheric carbon monoxide budget 2000–2017 inferred from multi-species atmospheric inversions. *Earth System Science Data*, *11*(3), 1411–1436. https://doi.org/10.5194/essd-11-1411-2019

Zhu, Q., Laughner, J. L., & Cohen, R. C. (2022). Estimate of OH trends over one decade in North American cities. *Proceedings of the National Academy of Sciences of the United States of America*, *119*(16), e2117399119. https://doi.org/10.1073/pnas.2117399119